Hydrodynamics of Particulate Motion in Sinusoidal Pores Via a Singularity Method

Axisymmetric motions of suspended spheres and dumbbells through sinusoidally corrugated capillaries are considered as an illustrative model of particulate or macromolecular transport in porous media. Numerical simulations are carried out using a least-squares singularity method, which is well suited to simulating creeping flows in the complicated, time-evolving geometries associated with particle motion through nonrectilinear pores. The numerical method is applied to a representative closure problem, whose solution yields effective transport coefficients describing particulate flow in porous media. With reference to polymer-induced mobility control in enhanced oil recovery, a hydrodynamic mechanism of mobility reduction is studied using a rigid dumbbell polymer model.

Ludwig C. Nitsche
Howard Brenner
Department of Chemical Engineering
Massachusetts Institute of Technology
Cambridge, MA 02139

Introduction

The hydrodynamics of suspended particles in porous media is relevant to a variety of natural and technological processes, including hindered diffusion in membranes (Deen, 1987), hydrodynamic chromatography (Brenner and Gaydos, 1977; Prud'homme and Hoagland, 1983; McHugh, 1984), deep bed filtration (Tien and Payatakes, 1979; Sharma and Yortsos, 1987b), and groundwater contamination (Corapcioglu et al., 1987). In the context of enhanced oil recovery it is of interest to be able to model emulsion flooding (McAuliffe, 1973; Schmidt et al., 1984) and polymer flooding (Gogarty, 1967; Chauveteau, 1982) processes—which are designed to achieve mobility control—as well as the movement of fines in porous rock (Sharma and Yortsos, 1987a,c). Accurate computation of particle mobilities in realistic models of tortuous media represents an essential element in the effective analysis of such phenomena.

As a model system, we simulate axisymmetric Stokes hydrodynamics of periodic particle trains moving within corrugated capillaries (Nitsche, 1989), using an extended boundary element technique (Mathon and Johnston, 1977) that has elements in common with the numerical singularity method employed by Dąbroś (1985). The general case of a multiparticle chain in each unit cell can be treated with our FORTRAN code. Example problems illustrate the utility of this numerical model in a mechanistic-hydrodynamic approach to the classes of transport phenomena cited above.

To be sure, a straight tube with periodic axial variations in radius represents a gross simplification of the exceedingly complex, disordered geometries of real porous microstructures. Nevertheless, as has been recognized in the past, the successive expansions and contractions embodied in this type of idealization capture essential physical features whose existence is central to a variety of transport phenomena in porous media. Payatakes et al. (1973) discuss how the complex interstitial geometry of granular beds can be translated into a description involving the concept of a *unit bed element,* which corresponds to one unit cell of a periodically constricted tube. Viewed as a *building block* for the overall understanding of specific pore-scale mechanisms, use of the corrugated capillary represents an effective modeling approach, for which ample precedent can be found in the literature: sinusoidal and otherwise periodically constricted capillaries have been used as geometrical idealizations in theoretical treatments of single-phase Newtonian flow through porous media in the Stokes (Tilton and Payatakes, 1984) and inertial (Payatakes et al., 1973; Deiber and Schowalter, 1979) regimes, non-Newtonian flow through porous media (Deiber and Schowalter, 1981; Phan-Thien and Khan, 1987),

Correspondence concerning this paper should be addressed to L. C. Nitsche, Department of Applied Mathematics and Theoretical Physics, University of Cambridge, Silver Street, Cambridge CB3 9EW, England.

dispersion in porous media (Hoagland and Prud'homme, 1985), capillary stability and displacement in pores (Giordana and Slattery, 1983, 1987), trickle flow (Sáez et al., 1986), and mass transfer (Fedkiw and Newman, 1977) in packed beds, as well as deep bed filtration (Payatakes et al., 1974; Tien and Payatakes, 1979).

Corrugated walls allow one to model effects—observed in real porous media—that fail to be captured by conventional cylindrical-tube idealizations (Scheidegger, 1974, Chap. 6) of pore structure. For example, *Lagrangian unsteadiness* plays an important role in viscoelastic flow through porous media; as a viable illustrative model, the problem of viscoelastic flow in corrugated tubes has received considerable attention from both numerical and experimental points of view (Deiber and Schowalter, 1981; Phan-Thien and Khan, 1987).

Closely related to the concept of Lagrangian unsteadiness, and central to the geometrically more complex phenomena embodied in particulate or multiphase flow through porous media, is the *evolution of the system through a family of (quasistatic) conformations*. The inherently *conformation-dependent* hydrodynamics of a train of particles moving along the axis, say, of a corrugated capillary has no counterpart in the case of a tube of uniform circular cross section (Wang and Skalak, 1969). One of the advantages of the present numerical method is the relative ease with which complicated interstitial geometries—particularly their evolution through different particle-wall configurations—can be treated.

The general numerical method and its implementation are described in the following two sections; details are provided in appendices A and B (see also Nitsche, 1989). Positioning of the hydrodynamic singularities is then considered, following which comparisons with existing numerical results obtained by alternate schemes (Tilton and Payatakes, 1984; Wang and Skalak, 1969) are presented for two test problems. These examples demonstrate the accuracy and versatility of the singularity method. Succeeding sections study the motion of spheres and dumbbells along the axis of sinusoidal capillaries. Applications of the computations to mean transport coefficients for suspended particles or macromolecules in pores are explored, along with the accuracy of an approximate approach—based upon hydraulic radius—for estimating mean particle velocities. Finally, in the case of rigid dumbbells the numerical simulations are used to decompose the flow hindrance effect into two hydrodynamic submechanisms: independent resistance, and linkage.

Description of the Numerical Scheme

Dabros (1985), who provides a review of singularity methods as applied to Stokes flow problems, advances a numerical scheme whereby a *discrete spatial distribution* of two fundamental solutions (point force, point source) *inside* solid particles is used to approximate the surrounding flow field, the strengths of these singularities being optimized with respect to the no-penetration, no-slip boundary conditions at particle surfaces. This approach, which has some elements in common with slender-body theory (Batchelor, 1970) contrasts with the method of multipole expansions (Gluckmann et al., 1971; Sangani and Acrivos, 1982), which is based upon systematically adding higher order *derivatives* (multipoles) of the basic singularity to the representation to improve the degree of approximation to which the boundary conditions are satisfied.

The traditional boundary element approach to numerical calculation of particulate Stokes flows involves a continuous distribution of singularities over the solid surfaces. Imposition of the boundary conditions then leads to an integral equation of the first or second kind for the distribution density, corresponding, respectively, to the use of single-layer or double-layer potentials in generating the solution (Youngren and Acrivos, 1975; Karrila and Kim, 1989). Singular integrals result from the necessity of evaluating the flow fields precisely on the surface(s) containing the generating singularities. An alternative that avoids singular integrals, and that has advantages for evaluating derivatives at the boundary (Han and Olson, 1987), is to put the singularities on a separate auxiliary boundary lying *behind* the solid surface(s), that is, inside the solid phase. Enforcement of the boundary conditions can be carried out by collocation (Patterson et al., 1985) or in a least-squares sense (Mathon and Johnston, 1977). A further refinement is embodied in incorporating the singularity *positions* in the boundary optimization along with their coefficients (Mathon and Johnston, 1977; Han and Olson, 1987). The resulting adaptive method reduces the number of singularities required to achieve a given level of accuracy; this feature must be weighed against the concomitant need for a more complicated nonlinear optimization (as well as new function evaluations each time the poles are moved in the iterative solution), a consideration explored by Mathon and Johnston. Here we use the fixed-singularity approach with least-squares stipulation of the boundary conditions. In principle this type of boundary element formulation is then essentially similar to Dąbroś's method, although there are distinctions, discussed below.

Karrila and Kim (1989) mention, but do not implement, the possibility of augmenting their boundary-integral technique with a Dąbroś-type scheme in the case of particles of large aspect ratio—prolate or oblate; axisymmetric problems would require ring singularities of the type considered here. Finally, we note that exact solutions of various exterior and interior Stokes flow problems have also been obtained (Chwang and Wu, 1975; Chwang, 1975) by suitable spatial distributions of singular and regular solutions.

In considering the case of a particle moving near a plane wall, Dąbroś (1985) used fundamental solutions satisfying no-penetration, no-slip conditions at the wall. Thus, only the boundary conditions on the sphere had to be considered in the optimization scheme for determining the singularity strengths. Similarly, in applications to spatially periodic media, both multipole (Sangani and Acrivos, 1982) and boundary integral (Zick and Homsy, 1982) approaches typically proceed by utilizing Hasimoto's (1959) periodic fundamental solutions. Although the idea of using singular solutions with some of the boundary conditions already built in can lead to simplifications in implementing the boundary optimization, this is offset somewhat by the more extensive computations required for these more complicated function evaluations. Rather than attempting to incorporate axial periodicity into the fundamental solutions, we opt instead to distribute singularities everywhere outside the fluid domain of the basic unit cell, treating *all* boundary conditions (including periodicity) in the least-squares optimization. Note that in this scheme one can position singularities even at locations where they would reside in the fluid (or solid) domain of *neighboring* unit cells: once the unit-cell boundary-value problem has been posed, events occurring outside of the fluid domain of interest are irrelevant.

Implementation of the Singularity Method

We proceed now with a dimensionless formulation of the relevant hydrodynamic problem. In this initial investigation we confine our attention to axisymmetric flows, utilizing circular cylindrical coordinates (r, z, ϕ). For the class of phenomena considered, no flow occurs in the angular direction, so that (r, z) coordinates and r and z components of velocity suffice for a complete description. (The azimuthal angle ϕ will enter, however, in constructing approximations to the axisymmetric ring singularities.)

In the nondimensional formulation of the hydrodynamical Stokes flow problem given below, the maximum tube radius is taken as unity. We denote by b the minimum tube radius (which is then the same as the constriction ratio) and by $2L$ the wavelength of the corrugations. Thereby, the sinusoidal tube wall is given by the equation

$$r = w(z) = \frac{1}{2}(1 + b) + \frac{1}{2}(1 - b)\cos\left(\frac{\pi z}{L} + 2\pi\varphi\right) \quad (1)$$

where φ specifies the translational position of the sinusoidal corrugations with respect to the plane $z = 0$. Thus, the unit cell $\tau(\varphi)$ is given by $0 \le r \le w(z)$, $-\mathcal{L} \le z \le \mathcal{L}$, with $\mathcal{L} = \mathcal{N}L$. Here, $\mathcal{N}$ is the number of wavelengths contained in the unit cell; one should take $\mathcal{N} > 1$ for computations involving particles longer than one wavelength, or in assessing the importance of end effects. In order to avoid (straightforward but more tedious) complications arising from intersections of the end faces $(z = \pm\mathcal{L})$ with solid particles, tracking of (axial) particle motion is carried out by keeping the particle (or multiparticle assemblage) roughly centered about $z = 0$ while varying φ. $\tau^{(\mathcal{F})}(\varphi)$ and $\tau^{(\mathcal{P})}(\varphi)$ refer, respectively, to the fluid- and solid-occupied subsets of $\tau(\varphi)$; $\tau^{(\mathcal{P})} = \bigcup_{k=1}^{K} \mathcal{P}_k$, with $\mathcal{P}_k$ the kth particle. We consider spheroidal particles whose symmetry axes are aligned along the corrugated tube axis, $r = 0$; α_k is the half-length of $\mathcal{P}_k$ with the axis, and β_k its maximum radius. Each particle $\mathcal{P}_k$ moves with velocity v_k along the axis. Let $\mathcal{S}^{(\mathcal{W})}$, $\mathcal{S}^{(\mathcal{P}_k)}$ $(k = 1, 2, \ldots, K)$ denote the tube wall and the particle surfaces, respectively. Furthermore, let $\mathcal{S}^+$ and $\mathcal{S}^-$ denote the respective cross sections $z = \mathcal{L}$ and $z = -\mathcal{L}$. Thereby, we have that

$$\partial\tau^{(\mathcal{F})} = \mathcal{S}^{(\mathcal{W})} \cup \left(\bigcup_{k=1}^{K} \mathcal{S}^{(\mathcal{P}_k)}\right) \cup \mathcal{S}^+ \cup \mathcal{S}^- \quad (2)$$

Stokes equations are posed (in dimensionless form) in the fluid domain $\tau^{(\mathcal{F})}$, together with no-penetration, no-slip conditions imposed at the solid surfaces, and periodicity conditions at the end faces of the unit cell. (Although we seek axisymmetric solutions, formulation of the governing equations in circular cylindrical coordinates is not directly relevant to the numerical method employed here. Thus, for the present we retain an invariant notation.)

$$\begin{aligned} \nabla^2\boldsymbol{u} &= \nabla p \\ \nabla \cdot \boldsymbol{u} &= 0 \end{aligned} \qquad \boldsymbol{r} \in \tau^{(\mathcal{F})} \quad (3)$$

$$\begin{aligned} \boldsymbol{u} &= 0 \qquad \text{on } \mathcal{S}^{(\mathcal{W})} \\ \boldsymbol{u} &= v_k \boldsymbol{e}_z \qquad \text{on } \mathcal{S}^{(\mathcal{P}_k)} \ (k = 1, \ldots, K) \end{aligned} \quad (4)$$

$$\boldsymbol{u}|_{z=\mathcal{L}} = \boldsymbol{u}|_{z=-\mathcal{L}}$$

$$\left.\frac{\partial}{\partial z}\boldsymbol{u}\right|_{z=\mathcal{L}} = \left.\frac{\partial}{\partial z}\boldsymbol{u}\right|_{z=-\mathcal{L}} \quad (5)$$

$$p|_{z=\mathcal{L}} - p|_{z=-\mathcal{L}} = \Delta p_0 \quad (6)$$

where Δp_0 is a prescribed constant.

Motivated by Dąbroś's (1985) approach, we utilize as our basis functions the point force (Stokeslet) and point source. The solution we seek is axisymmetric, with zero angular velocity component, $u_\phi = 0$. Thus, in a representation utilizing circular cylindrical coordinates, each singularity point (r_n, z_n) $(n = 1, 2, \ldots, N)$ is associated with a continuous, uniform distribution of singularities around a circle centered on the z axis (Karrila and Kim, 1989). The actual numerical calculations are carried out using a finite number $(2J)$ of singularities distributed with even spacing in the azimuthal direction; a large number of these angular subdivisions will lead to a good approximation of the corresponding ring singularity. Note that this type of computation would correspond to the application of a three-dimensional singularity method to the special case of an axisymmetric flow.

There exists but one kind of ring-source solution (referred to here with a superscript [3]), but we utilize *two* types of ring-force solutions ([1] and [2]), corresponding, respectively, to *radial* and *axial* forces at each position along the ring. Details of the evaluation of the axisymmetric flow fields $v_r^{[i]}(r, z, r_n, z_n)$, $v_z^{[i]}(r, z, r_n, z_n)$, and $p^{[i]}(r, z, r_n, z_n)$ for these singular solutions are given in Appendix A.

Ring singularities alone give good results (Nitsche, 1989). However, in the interests of greater generality, it is perhaps of interest to consider the limit as the radius of the singularity ring tends to zero, for which limit one then observes that

(i) radial-force solution $\longrightarrow 0$

(ii) axial-force solution $\longrightarrow$ point force

(iii) ring source $\longrightarrow$ point source

The option of distributing singularities along the axis should be of particular interest in treating the motion of slender bodies (Batchelor, 1970) and is incorporated (with variable discrete lineal density) into the FORTRAN code. (Of course, these singularities must reside outside the fluid domain. They can be chosen to lie inside the particle(s) or beyond the end faces $z = \pm\mathcal{L}$.) Note, however, that collapse of the radial-force singular solution as $r_n \longrightarrow 0$ renders the corresponding coefficients (Eq. 8, below) irrelevant; as will be discussed in Appendix B, these degenerate columns are removed from the least-squares matrix. (Alternately, one could view this as an opportunity to introduce further hydrodynamic singularities to take the place of the degenerate radial-force solutions.)

Finally, use is also made of one kind of regular solution—a parabolic velocity profile, corresponding to a hypothetical ghost cylinder of radius a:

$$U(r) = \left(\frac{r^2}{a^2} - 1\right) \quad (7)$$

In the subsequent calculations, a is chosen to lie between the minimum and maximum tube radii, that is, $b \le a \le 1$. This solution is of particular utility in dealing with a circular

cylindrical tube (Wang and Skalak, 1969), for which we take $a = b = 1$.

The velocity and pressure fields are expressed as linear combinations of the individual contributions from ring singularities located at the points (r_n, z_n), $n = 1, 2, \ldots, N$ together with the parabolic profile; the coefficients $G_n^{[i]}$, A in the expressions appearing below are, as yet, unknown:

$$\begin{aligned} u_r(r,z) &= \sum_{i=1}^{3}\sum_{n=1}^{N} G_n^{[i]} v_r^{[i]}(r,z,r_n,z_n) \\ u_z(r,z) &= U(r) + \sum_{i=1}^{3}\sum_{n=1}^{N} G_n^{[i]} v_z^{[i]}(r,z,r_n,z_n) \\ p(r,z) &= 4(A/a^2)z + \sum_{i=1}^{3}\sum_{n=1}^{N} G_n^{[i]} p^{[i]}(r,z,r_n,z_n) \end{aligned} \tag{8}$$

To impose periodicity of the velocity fields, one also needs to obtain formulas for the z derivatives $\partial u_r/\partial z$ and $\partial u_z/\partial z$; these are given in Appendix A.

By construction, the above velocity and pressure fields satisfy the Stokes equations. They are also (to a good approximation for large J) axisymmetric. It remains to choose the coefficients $G_n^{[i]}$ ($i = 1, 2, 3$; $n = 1, 2, \ldots, N$) and A so as to optimize the degree of satisfaction of the no-penetration, no-slip boundary conditions, Eqs. 4, imposed at solid surfaces (corrugated tube wall, particle surfaces), as well as of the periodicity, Eqs. 5, and pressure drop, Eq. 6, conditions imposed at the ends of the unit cell ($z = \pm\mathcal{L}$). For this purpose we use a least-squares criterion involving a summation over residuals evaluated at discrete points on the boundaries, which corresponds to the following integral quantity:

$$\begin{aligned} &\int_{\mathcal{W}} [u_r^2 + u_z^2]\, dS + \sum_{k=1}^{K} \int_{\mathcal{P}_k} [u_r^2 + (u_z - v_k)^2]\, dS \\ &+ \int_{\mathcal{E}} [(u_r^+ - u_r^-)^2 + (u_z^+ - u_z^-)^2 + (\partial u_r/\partial z^+ - \partial u_r/\partial z^-)^2 \\ &\quad + (\partial u_z/\partial z^+ - \partial u_z/\partial z^-)^2 + (p^+ - p^- - \Delta p_0)^2]\, dS \end{aligned} \tag{9}$$

The boundary points are indexed by m; to each is assigned a weight ρ_m which corresponds to Simpson's rule for approximating the above axisymmetic integral.

Tube wall, $\mathcal{W}$:	$(r_m^{(\mathcal{W})}, z_m^{(\mathcal{W})})$, $\rho_m^{(\mathcal{W})}$	$(m = 1, 2, \ldots, M^{(\mathcal{W})})$
End-cap ($z = \mathcal{L}$), $\mathcal{E}$:	$(r_m^{(\mathcal{E})}, z_m^{(\mathcal{E})})$, $\rho_m^{(\mathcal{E})}$	$(m = 1, 2, \ldots, M^{(\mathcal{E})})$
Particle k, $\mathcal{P}_k$:	$(r_m^{(\mathcal{P}_k)}, z_m^{(\mathcal{P}_k)})$, $\rho_m^{(\mathcal{P}_k)}$	$(m = 1, 2, \ldots, M^{(\mathcal{P}_k)})$

In each calculation we specify the sphere velocities v_k ($k = 1, 2, \ldots, K$) and pressure drop Δp_0. The numerical method then consists of a linear least-squares optimization of the coefficients, $G_n^{[i]}$ ($i = 1, 2, 3$; $n = 1, 2, \ldots, N$) and A with respect to the boundary conditions. Implementation of the scheme using a LINPACK QR algorithm (Dongarra et al., 1979) is detailed in Appendix B. For a given arrangement of singularities the total number of boundary stipulations ($2M^{(\mathcal{W})} + 5M^{(\mathcal{E})} + 2\sum_{k=1}^{K} \cdot M^{(\mathcal{P}_k)}$) was between 2.5 and 4 times as large as the number of coefficients ($3N + 1 - N_{\text{axis}}$, where N_{axis} is the number of singularities lying on the z axis).

As will be utilized subsequently, any flow can be expressed as a linear combination of the following K + 1 base cases:

- Case 0: $\Delta p_0 = \Delta P_0, v_k = 0$ $(k = 1, 2, \ldots, K)$
- Case k, $k = 1, 2, \ldots, K$: $\Delta p_0 = 0, v_k = 1, v_j = 0$ $(j \neq k)$

where cases 1, 2, ..., K result in a resistance matrix (Happel and Brenner, 1983) for axial motions. This general type approach was discussed by Dabroś (1985), ultimately to be rejected in favor of a direct method for calculating the particle motions in an arbitrary three-dimensional flow field, with force and torque constraints for each particle incorporated into the boundary optimization. Within the axisymmetric context considered here, for which only one variable (axial velocity v_k) characterizes the instantaneous motion of each particle, stored hydrodynamic coefficients provide a convenient mode of studying different flow conditions in later sections of this paper. Note that the prescribed pressure drop and particle velocities appear only on the righthand side of the linear least-squares problem (Appendix B). Thus, for each geometry, generation of the least-squares matrix and the QR decomposition need to be carried out but once (Dabroś, 1985).

No net force is associated with a radial-force or source ring singularity. Thus, the total external force F_k exerted (in the axial direction) upon any particle $\mathcal{P}_k$ is just the sum of the strengths $G_n^{[2]}$ corresponding to those singularities (r_n, z_n) lying inside of $\mathcal{P}_k$ (Chwang and Wu, 1975).

Remark: Here, we actually impose the boundary conditions, Eqs. 4–6, only at one azimuthal angle ($\phi = 0$); the boundary condition optimization scheme assigns each discrete point on the corresponding *curves* a weight consistent with Simpson's rule for approximating *axisymmetric* surface integrals. Only if the singular solutions were exactly axisymmetric, would the condition in Eq. 9 be exact. Thus, if one views the ring summation over discrete azimuthal angles ($\phi_j, j = 1, 2, \ldots, 2J$) merely as representing an approximate *quadrature* of the corresponding *integral* representation formulas for the singular solutions, then it would appear to be essential for the ring summation to converge more or less completely before the function values are used in the boundary optimization. In particular, one should be able to compute the matrix entries so accurately (requiring sufficiently large J) that the corresponding *individual coefficients* $G_n^{[i]}$ computed by the QR algorithm are insensitive to further increases in J. It should be noted in this connection that a uniformly weighted summation over evenly spaced angles around the ring—corresponding to the trapezoid rule for approximating complete elliptic integrals (Appendix A)—gives *exponential* convergence with increasing number of subdivisions, as is well known. Indeed, $J = 18$ was found to be sufficient for the coefficients $G_n^{[i]}$ to settle down, at least to a significant degree, in the case of the single-phase flow calculations given later using the SM1 parameter set, Table 1. In some cases, however, it was observed that even very large values of J, leading to undesirably high computation times, would be needed for convergence of the individual coefficients $G_n^{[i]}$. This is most likely due to ill conditioning of the rectangular matrix.

Nevertheless, very accurate numerical solutions can be obtained at moderate values of J at which the $G_n^{[i]}$ have not yet fully converged. This is explained by the following line of reasoning: What is actually generated by the ring summations is a solution which, while not exactly axisymmetric, possesses discrete $2J$-fold rotational symmetry about the tube axis. Beyond some critical value of J (for a given mesh of singularities and boundary points), the inexactness associated with the azimuthal discretization becomes smaller than the accuracy limitation of the mesh itself. As $J \to \infty$ with a fixed mesh, it seems likely that the computed *flow fields* u_r, u_z, and p should converge more quickly than the individual coefficients $G_n^{[i]}$. In the calculations involving

Table 1. Parameters for Ring Summation, Singularity Positions, and Boundary Discretization, Illustrated in Figures 1, 2, 5

Designation	Ring Sum., J	Singularities			Boundary Points			Computation Time, min.†		
		Wall	End-cap	Particle	$M^{(\mathcal{W})}$	$M^{(\mathcal{E})}$	$M^{(\mathcal{P}_k)}$	$K=0$	$K=1$	$K=2$‡
SM1	18	1 row × 15	1 col × 9	—	65	45	—	<2	—	—
SM2	30	1 row × 15	1 col × 9	1 arc × 9	65	45	55	—	<4	<6
SM3	60	1 row × 31	1 col × 17	1 arc × 17	115	85	95	—	<26	—
SM4*	180	5 rows × 9	3 cols × 5	3 arcs × 9	115	85	95	—	~90	~130

*The program used for the SM4 calculation parameters differed slightly in the singularity placement subroutine from that used for SM1–SM3, although both versions offered the choice of areal or lineal distribution of the singularities

†Typical UNIX 'user' times when running the programs on a Sun SPARCstation 1

‡These runs include supplementary computations for the empty tube and for only one sphere present; see Appendix B

suspended particles, rather good convergence of the flow fields—checked over the unit cell face ($z = \mathcal{L}$) cross section—was obtained using $J = 30$ with the SM2 set of parameters, Table 1. Mesh refinement of the singularities and boundary points should be accompanied by an appropriate increase in J. Larger values of J were also needed close to the lubrication limit. Although the present formulation is for axisymmetric flows, the above information may be useful for estimating how many angular subdivisions would be required in a fully three-dimensional implementation of the singularity method, will be developed.

Positioning of the Hydrodynamic Singularities

In implementing his numerical singularity scheme, Dąbroś (1985) used three-dimensional clustering of relatively small numbers of singularities, for example, seven or thirteen singularities arranged in a six-armed star shape. Given that closely packed basic singularities can approximate higher order singularities inside the particles—somewhat in line, then, with the method of multipoles—this approach has appeal for seeking good estimates with a small number of singularities (when interparticle separations are not too small), which was the main emphasis of the Dąbroś paper. In order to develop a mesh refinement scheme for applying the method to more complicated geometries, it would be desirable to avoid three-dimensional discretization. (For the present axisymmetric problem, the notions of volumetric and areal discretization must be replaced by their respective areal and lineal counterparts.) This is where the boundary-element character of the method becomes useful; for, one actually needs only to refine a mesh whose dimension equals that of the boundary (Mathon and Johnston, 1977).

Experience with fixed-singularity methods suggests that the poles should be placed fairly close to the surfaces (or curves) on which the boundary conditions are specified. This rule of thumb stems from considerations of matrix conditioning (Mathon and Johnston, 1977) as well as the desire to resolve curvature in the boundary (Patterson et al., 1985). It is thus interesting to note that in nonlinear adaptive schemes which optimize the singularity positions, the poles often tend to move away from the boundary as the iteration proceeds, and can sometimes even seem to migrate toward infinity (Han and Olson, 1987). In view of these observations, we tried both one- and two-dimensional discretization, but found the former to be more robust in addition to its advantage for ease of implementation.

We shall use the designations SM1 through SM4 to refer to the respective sets of calculation parameters listed in Table 1. The corresponding spatial arrangements of poles are illustrated in subsequent figures.

Two Test Problems for the Numerical Method

Single-phase flow through a sinusoidal tube

The problem of single-phase creeping flow through a sinusoidal tube was treated numerically by Tilton and Payatakes (1984) using a collocation method. Dimensionless tabulations were presented of the pressure drop ΔP_1^* (occurring over one unit cell) vs. maximum tube radius r_2^* and constriction ratio r_1^*/r_2^*. In terms of the present notation these dimensionless parameters are respectively given by

$$r_2^* = \frac{1}{2L'} \quad \frac{r_1^*}{r_2^*} = b, \quad \Delta P_1^* = -\frac{2\pi b^2 L \Delta p_0}{Q\mathcal{N}}$$

Our numerical approach was applied to this same problem. (In applying the general programs to test cases, we did not take advantage of fore–aft symmetry.) For $r_2^* = 0.5$, Table 2 compares values of ΔP_1^* vs. r_1^*/r_2^*, obtained using the calculation parameters SM1, with those of Tilton and Payatakes (T&P). The computations were carried out using $\varphi = 0$ for the geometric phase variable, Figure 1. (The geometric phase variable φ, Eq. 1, is not to be confused with the azimuthal angle ϕ.) This choice was advantageous because it led to a high density of poles near the constrictions—where they would seem to be needed most to resolve the converging-diverging flow field. It was found, for example, that choosing $\varphi = 0.5$ (constriction in the middle of the unit cell) did not work as well for $r_1^*/r_2^* = 0.1$ with the SM1 parameters. As can be seen from the tabulated values, excellent results are obtained for all constriction ratios r_1^*/r_2^* with remarkably few singularities.

Table 2. Results from Current Singularity method and from Tilton and Payatakes (1984) for Single-Phase Flow in a Sinusoidal Capillary, $r_2^* = (2L)^{-1} = 0.5$

r_1^*/r_2^*	ΔP_1^*	
	T&P	SM1
0.1	400.0	399.7
0.2	165.0	165.0
0.3	101.1	101.0
0.4	72.18	72.17
0.5	55.99	55.99
0.6	45.88	45.88
0.7	39.28	39.28
0.8	35.08	35.08
0.9	32.74	32.74
1.0	32.00	—

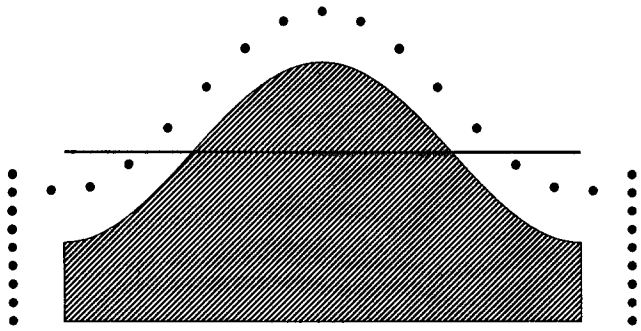

Figure 1. Singularity positions (SM1) for calculating flow fields in single-phase flow through a sinusoidally corrugated pore.

$b = 0.3$; $L = 1.0$; $\varphi = 0.0$

Horizontal line indicates radius of ghost cylinder on which parabolic velocity field vanishes

It should be pointed out that although the centerline fluid velocity is exactly twice the mean fluid velocity in Poiseuille flow through a cylindrical tube, the *time-average* velocity of centerline fluid elements *exceeds* twice the volume-average fluid velocity if the tube has corrugations. (It can be shown that the volume average of the fluid velocity over one unit cell is the same as the long-time mean velocity of a tagged fluid molecule undergoing Brownian motion [Brenner, 1980].) This feature is quantified by Table 3 and is considered again in succeeding sections.

Spatially periodic train of suspended spheres in a circular tube

Wang and Skalak (1969) studied hydrodynamic problems involving a periodic train of axially centered spheres in a circular cylindrical tube. To obtain the stream function, they began by writing two series solutions each of which was periodic, was regular within the fluid domain, and satisfied the boundary conditions at the tube wall. The desired solution was expressed as a linear combination of these solutions together with higher derivatives, in a manner analogous to the multipole approach.

Table 3. Ratio of Time-Average Velocity of Centerline Fluid Elements* to Volume-Average Fluid Velocity as a Function of Constriction Ratio† for Single-Phase Stokes Flow through a Sinusoidal Capillary, $r_2^* = (2L)^{-1} = 0.5$**

r_1^*/r_2^*	$\dfrac{\langle u_z\{r=0\}\rangle_\tau^0}{\langle u\rangle_\tau^0}$
0.1	4.760
0.2	4.073
0.3	3.493
0.4	3.030
0.5	2.676
0.6	2.412
0.7	2.223
0.8	2.096
0.9	2.024

* $\langle u_z\{r=0\}\rangle_\tau^0$

** $\langle u\rangle_\tau^0$

† $b = r_1^*/r_2^*$

Satisfaction of the boundary conditions on the sphere surfaces led to an infinite system of linear algebraic equations for the unknown coefficients; this system was truncated to obtain numerical values.

Results were tabulated for three types of flow:

(i) Pressure driven flow (discharge $\pi V/2$) past stationary spheres in the tube—described by a drag coefficient K_V and pressure drop coefficient P_V

(ii) Sedimentation, that is, motion of the spheres (velocity U) with no net discharge—described by a drag coefficient K_U and pressure drop coefficient P_U

(iii) Neutrally buoyant spheres carried along by the fluid, that is, no net hydrodynamic force (or torque) on each sphere—described by the ratio $2U/V$ of sphere velocity to mean mixture velocity and by the pressure gradient coefficient G_{V0}.

Below we indicate the relation between Wang and Skalak's (1969) dimensionless variables and ours, for the case of a single sphere ($\beta = \alpha$) in a circular cylindrical ($b = 1$) unit cell.

	Wang and Skalak (1969)		Present Notation	
Geometry	λ	β	$\alpha = \alpha_1$	$2\mathcal{L}$
Velocities	U	V	v_1	$2Q/\pi$
(i) Fixed spheres	K_V	P_V	$-F_1/12\alpha Q$	$-(\pi\Delta p_0/2Q) - 8\mathcal{L}$
(ii) Sedimentation	K_U	P_U	$F_1/6\pi\alpha v_1$	$\Delta p_0/v_1$
(iii) Freely suspended	$2U/V$	G_{V0}	$\pi v_1/Q$	$-(\pi\Delta p_0/16Q\mathcal{L}) - 1$

Table 4 compares results derived from our singularity method (SM2 and SM4) with those of Wang and Skalak (W&S). To avoid confusion involving geometric parameters, their dimensionless coefficients are presented as functions of our variables α and $\mathcal{L}$. Positioning of singularities for the various calculation parameters is as illustrated in Figure 2. Lineal distribution of singularities with roughly even spacing around the perimeter works very well with relatively few singularities (SM2) as long as the particle–wall gap is not too small ($\alpha \leq 0.6$). The more extensive, two-dimensional singularity mesh (SM4) gives better results near the lubrication limit. Uniform refinement of the lineal singularity distribution (from SM2 to SM3) also improves the accuracy of the computed coefficients for α near unity, as is indicated in Table 5.

Results for the above two test problems demonstrate the utility, accuracy, and versatility of the least-squares singularity method as applied to Stokes flow problems (see also Dabros, 1985; Nitsche, 1989). The combination of corrugated walls *and* suspended particles represents a significant complication, which arises, for example, in calculating particle trajectories for filtration models (Payatakes et al., 1974). Our investigation does not consider off-axis particle motion; nevertheless, the axisymmetric case embodies crucial features of particulate and macromolecular flow in porous media. Two illustrative calculations are discussed below.

Numerical Calculation for a Periodic Train of Spheres Moving within a Sinusoidal Capillary

The hydrodynamics of suspended matter moving through tortuous pores represents an important element in the effective description of such processes as deep bed filtration (Payatakes et al., 1974; Tien and Payatakes, 1979) and fines migration

Table 4. Results from Current Singularity Method (SM2, SM4) and from Wang and Skalak (1969) for a Periodic Train of Spheres Centered Along the Axis of a Circular Cylindrical Tube; $\mathcal{L} = 1.0$

α	W&S	SM2	SM4	W&S	SM2	SM4
	K_U			P_U		
0.1	1.263	1.263	1.263	1.506	1.506	1.506
0.2	1.679	1.679	1.679	3.922	3.922	3.922
0.3	2.368	2.368	2.368	8.018	8.018	8.018
0.4	3.585	3.585	3.586	15.41	15.41	15.41
0.5	5.929	5.929	5.930	29.86	29.86	29.87
0.6	11.04	11.04	11.04	61.65	61.64	61.67
0.7	24.52	24.45	24.56	145.6	145.2	145.8
0.8	73.90	71.20	74.43	451.7	435.7	454.9
0.9	440.0	285.4	469.1	2700	1762	2874
	K_V			P_V		
0.1	1.255	1.255	1.255	1.496	1.496	1.496
0.2	1.634	1.634	1.634	3.821	3.820	3.820
0.3	2.227	2.227	2.227	7.560	7.560	7.560
0.4	3.210	3.210	3.210	13.88	13.88	13.88
0.5	4.977	4.977	4.978	25.33	25.33	25.33
0.6	8.562	8.561	8.566	48.49	48.48	48.51
0.7	17.34	17.30	17.36	104.5	104.3	104.7
0.8	47.06	45.54	47.38	291.3	282.3	293.2
0.9	250.0	166.1	266.1	1500	1034	1640

	$2U/V$			G_{V0}		
α	W&S	SM2	SM4	W&S	SM2	SM4
0.1	1.987	1.987	1.987	0.1016×10^{-4}	0.09988×10^{-4}	0.1000×10^{-4}
0.2	1.947	1.947	1.947	0.320×10^{-3}	0.3198×10^{-3}	0.3203×10^{-3}
0.3	1.881	1.881	1.881	0.2438×10^{-2}	0.2435×10^{-2}	0.2438×10^{-2}
0.4	1.791	1.790	1.790	0.00999	0.01036	0.01037
0.5	1.679	1.679	1.679	0.03235	0.03231	0.03235
0.6	1.551	1.551	1.551	0.0840	0.08394	0.08406
0.7	1.414	1.415	1.414	0.1961	0.1967	0.1972
0.8	1.274	1.279	1.273	0.455	0.4475	0.4543
0.9	1.14	1.164	1.135	1.2	1.106	1.206

(Sharma and Yortsos, 1987a, c). Although modeling of entrainment and deposition using axisymmetric pores would entail off-axis motion, useful information on wall effects affecting transport *through* the pores can be obtained from the present axisymmetric calculations.

Owing to adsorbed surface impurities, droplets frequently behave hydrodynamically like solid spheres (Levich, 1962; chap. VIII). Thus, the results obtained here for *rigid* spheres may also apply to certain aspects of *fluid* particle transport, for example, in the context of emulsion flooding (Schmidt et al., 1984).

For a centerline train of spheres in a sinusoidal tube (Nitsche, 1989) we show explicitly how the mean disperse-phase velocity results from an integration over configurations through which the system passes (Giordano and Slattery, 1987). Simulations of this type could be combined with statistical distributions of pore and particle geometric parameters to yield results representative of real (disordered) media; see Payatakes et al. (1973) and Payatakes and Neira (1977) for modeling of granular porous media.

Calculations for this section and the next (on dumbbell movement) were carried out using the SM2 and SM4 parameter sets. Virtually identical results were obtained for the configuration-specific hydrodynamic quantities discussed below. Moreover, the pointwise flow fields (checked over the $z = \mathcal{L}$ cross section) were resolved with good accuracy using remarkably few singularities (SM2). Diagrams of the singularity positions will be shown for the dumbbell calculations in the next section.

In presenting results for the unit cell simulations, the position of the sphere (radius $\alpha_1 = 0.3$) relative to the wall corrugations ($b = 0.6, L = 1.0$) is given by the phase variable φ ($0 \le \varphi < 1$), with $\varphi = 0$ corresponding to spheres centered in the pore bodies. This convention means that $z_1^c = 0$ in the calculations involving one sphere in the unit cell. It was possible to save computer time by obtaining some of the single-sphere results as by-products of the two-sphere computations reported in the next section; details of this implementation appear in Appendix B. In these cases, $z_1^c = 0.5$, so that a shift in φ was needed for consistency with the above convention.

All configuration-specific hydrodynamic quantities are periodic functions of φ of period unity. In the calculations discussed below, the system depicted in Figure 3 is frozen in 20 quasistatic configurations, $\varphi_i = i/20$, ($i = 0, 1, \ldots, 19$). Owing to the presence of symmetries, explicit computations only have to be carried out for $0.00 \le \varphi \le 0.50$.

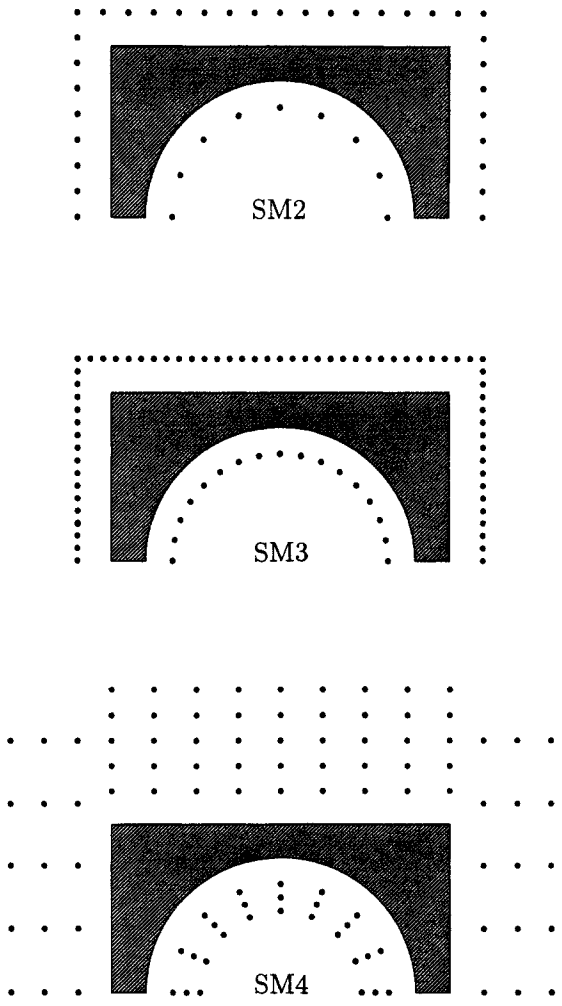

Figure 2. Singularity positions for the problem of spheres moving along the axis of a circular cylindrical tube.

$\alpha = \alpha_1 = 0.8; \mathcal{L} = 1.0; \varphi = 0.0$

Configuration-specific hydrodynamic quantities

To consider the additional flow resistance associated with the freely suspended spheres, Figure 4a displays dimensionless flow rate Q (normalized with repect to the empty-tube value $Q_0 = 0.4930$ for the same pressure drop $-\Delta p_0 = 10.0$) as a function of φ. Observe that even in the presence of converging and diverging flow fields, suspended spheres whose diameters are half as large as the throat diameter do not greatly reduce the total flow rate (Wang and Skalak, 1969). The greatest reduction in flow rate occurs not when the particles are centered in the constrictions, but rather when the particles reside *between* the throats and bodies. Since dissipation due to suspended particles arises from the inhomogeneity of the undisturbed flow field over their surfaces, this result is to be expected in view of the lack of axial velocity gradients at both the throats and bodies for flow in the empty tube. Rationalizing from a slightly different point of view, observe that the sphere velocity has zero component normal to the nearest section of the tube wall only when the sphere is centered in the constriction or in the body. Thus, the greatest hydrodynamic resistance—and hence the minimum instantaneous flow rate—is expected to occur somewhere in between. In the next section this flow hindrance effect will be seen to be substantially magnified in the case of suspended dumbbells.

Figure 4b shows the dependence of sphere velocity v_1 upon φ

Table 5. Mesh Refinement for Closely Fitting Spheres ($\alpha = 0.8, 0.9$) in Wang and Skalak (1969) Problem

	W&S	SM2	SM3	SM4
		$\alpha = 0.8, \mathcal{L} = 1.0$		
K_U	73.90	71.20	74.42	74.43
P_U	451.7	435.7	454.8	454.9
K_V	47.06	45.54	47.38	47.38
P_V	291.3	282.3	293.2	293.2
$2U/V$	1.274	1.279	1.273	1.273
G_{V0}	0.455	0.4475	0.4542	0.4543
		$\alpha = 0.9, \mathcal{L} = 1.0$		
K_U	440.0	285.4	467.3	469.1
P_U	2700	1762	2864	2874
K_V	250.0	166.1	265.2	266.1
P_V	1500	1034	1635	1640
$2U/V$	1.14	1.164	1.135	1.135
G_{V0}	1.2	1.106	1.203	1.206

Refer to Table 1 and Figure 2 for details of calculation parameters.

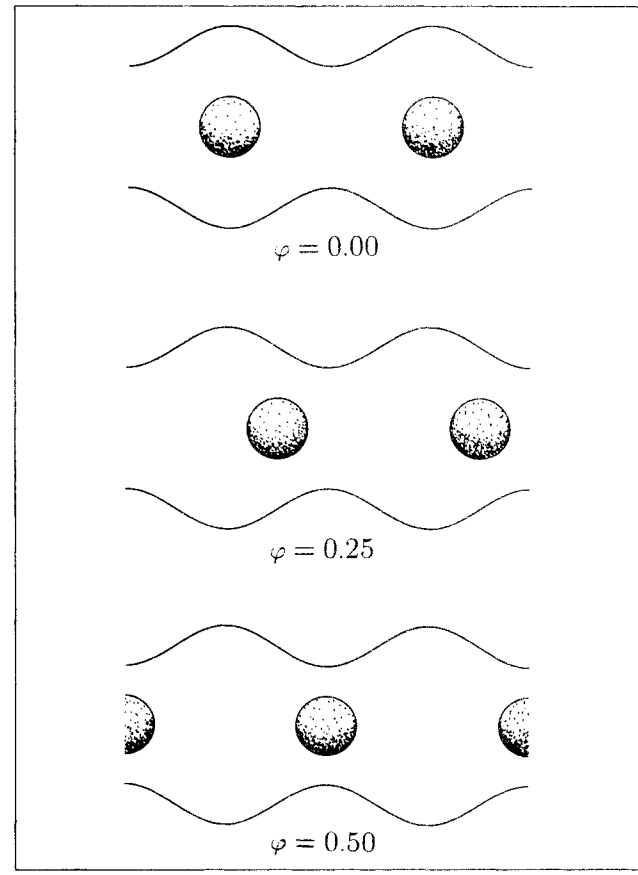

Figure 3. Idealized model involving the motion of spheres along the axis of a sinusoidally corrugated pore.

$\alpha_1 = 0.3; b = 0.6; L = 1.0$

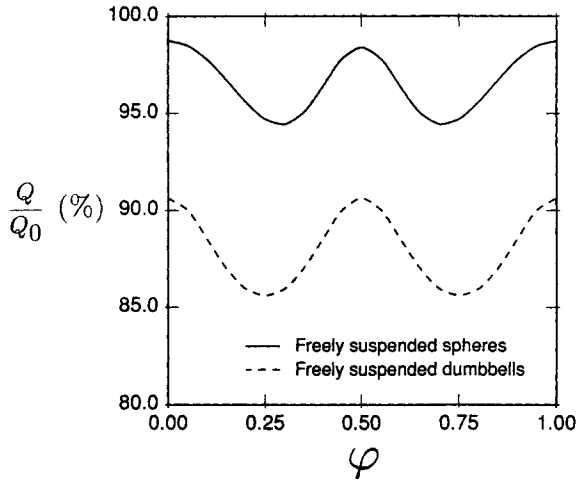

Figure 4. Configuration-specific hydrodynamic quantities for model system in Figure 3.
(a) Normalized total flow rate Q/Q_0 vs. φ for freely suspended spheres and dumbbells.
Q_0 is flow rate for single-phase flow driven by the same mean pressure gradient. Model system involving suspended dumbbells is shown in Figure 5.

for freely suspended spheres; a corresponding graph for the *sedimentation* case (force-driven particle motion with no net discharge) appears in Figure 4c.

The present calculation can be viewed as a particular model for implementing closure (Whitaker, 1986; Jiang et al., 1987) in deducing macroscopic phenomenological coefficients for an average macrocontinuum description of two-phase transport in porous media. To obtain coarse-grained velocities of each phase (fluid, particulate), we first perform a volume average over the unit cell. Here, we construct volume averages based upon total pore volume; note that in a porous medium modeled as a bundle of sinusoidal capillaries, these values must then be multiplied by

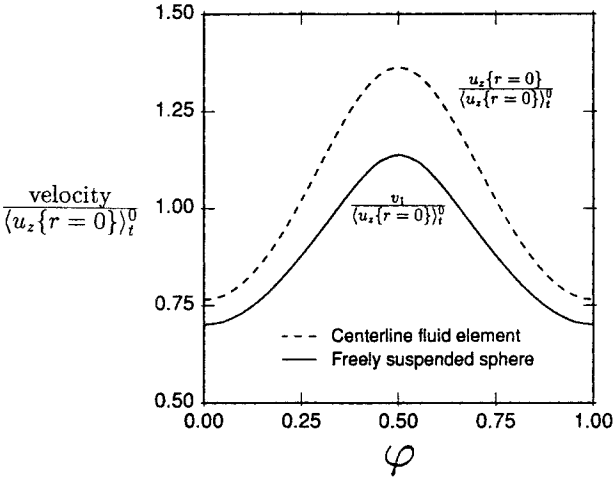

Figure 4b. Velocity $v_1(\varphi)$ of freely suspended spheres compared with velocity $u_z\{r=0\}(\varphi)$ of centerline fluid elements for single-phase flow driven by the same mean pressure gradient.
Both quantities are normalized with respect to time-average value $\langle u_z\{r=0\}\rangle_t^0$

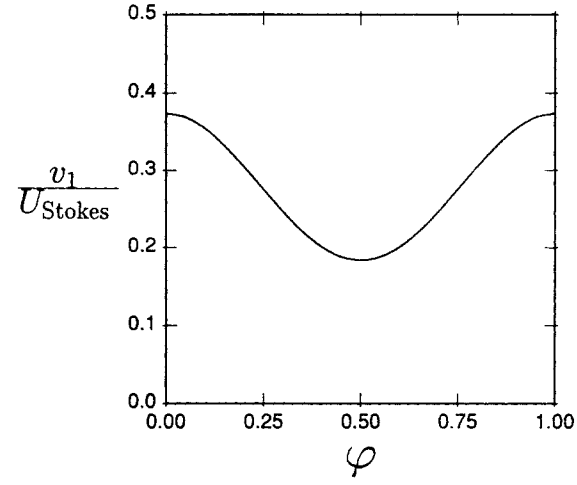

Figure 4c. Sphere sedimentation velocity normalized with respect to Stokes law velocity for the same applied force on one sphere.

the porosity to obtain superficial velocities based on total cross-sectional area of the porous-fluid-particulate mixture.

A two-dimensional integration of the axisymmetric velocity field with respect to both r and z can be avoided by invoking the identity $\boldsymbol{u} = \nabla \cdot (\boldsymbol{ur})$ (which follows from fluid incompressibility as expressed by the solenoidal nature of the velocity field, Eq. 3) and subsequently using the divergence theorem to convert the volume integrals over $\tau^{(\mathcal{F})}$ and $\tau^{(\mathcal{P})}$ into equivalent surface integrals over their bounding surfaces (Nitsche and Brenner, 1989), Eq. 2. Thereby we obtain the following expressions, where scalar variables suffice for the average velocities, which must lie parallel to the axis.

$$\langle u^{(\mathcal{F})}\rangle_\tau(\varphi) = \frac{1}{|\tau|}\left[2Q(\varphi)\mathcal{L} - \sum_{k=1}^{K} v_k(\varphi)\mathcal{V}_k\right]$$

$$\langle u^{(\mathcal{P})}\rangle_\tau(\varphi) = \frac{1}{|\tau|}\sum_{k=1}^{K} v_k(\varphi)\mathcal{V}_k \qquad (10)$$

with $|\tau| = \pi\mathcal{L}(3 + 2b + 3b^2)/4$ and $\mathcal{V}_k = (4/3)\pi\alpha_k\beta_k^2$. In the present example the instantaneous velocity $v_1(\varphi)$ corresponds to the configuration-specific *intrinsic* phase-averaged velocity (Whitaker, 1973; Jiang et al., 1987) of the particulate phase, that is, the volume average based upon particle volume; $\langle u^{(\mathcal{P})}\rangle\tau(\varphi) = \Phi^{(\mathcal{P})}v_1(\varphi)$ with $\Phi^{(\mathcal{P})}$ the particle volume fraction in the pore space.

Time-average hydrodynamic quantities

Multiphase (e.g., particulate) flow processes in porous media are inherently time dependent, as has been illustrated above with reference to a specific example. (For the class of quasistatic flows addressed here, time enters only as a parameter that indexes the geometric configurations through which the system evolves.) These temporal variations would generally not be discernible on the macroscopic scale; hence the motivation for temporal averaging in addition to spatial averaging in dealing theoretically with multiphase systems (Drew, 1971).

Time-average properties are obtained by integrating the quasistatic results over one period T of the time-periodic motion.

The procedure here parallels that employed by Giordano and Slattery (1987) in modeling displacements in sinusoidal capillaries. The integration over time is converted into one over the phase variable φ by considering the motion of the spheres over the distance $2\mathcal{L}$:

$$dz = 2\mathcal{L}d\varphi = v_1 dt \tag{11}$$

Thus,

$$\int_0^T (\ldots)\, dt \equiv 2\mathcal{L} \int_0^1 \frac{(\ldots)}{v_1} d\varphi \tag{12}$$

so that the time average $\langle f \rangle_t$ of any configuration-specific quantity $f(\varphi)$ can be expressed in the form (Giordano and Slattery, 1987)

$$\langle f \rangle_t = \frac{1}{\mathcal{C}} \int_0^1 \frac{f(\varphi)}{v_1(\varphi)} d\varphi \tag{13}$$

with

$$\mathcal{C} = \int_0^1 \frac{d\varphi}{v_1(\varphi)} \tag{14}$$

The volume- and time-averaged velocities for the above calculations are as follows:

$$\langle \langle u^{(\mathcal{F})} \rangle_\tau \rangle_t = 0.909 \langle u \rangle_\tau^0$$
$$\langle \langle u^{(\mathcal{P})} \rangle_\tau \rangle_t = 0.057 \langle u \rangle_\tau^0 \tag{15}$$

with $\langle u \rangle_\tau^0$ the volume-average fluid velocity corresponding to single-phase flow through the sinusoidal capillary driven by the same mean pressure gradient. Thus, the above numerical coefficients are, in the present context of disperse, two-phase flow, analogous to relative permeabilities for immiscible fluid–fluid flow through porous media (Scheidegger, 1974, Chap. 10).

The *kinematical interpretation* of averaged velocities has been discussed in detail by Nitsche and Brenner (1989) for periodic media, which analysis would be applicable to the present case for a porous medium idealized as a bundle of corrugated capillaries. Beyond an intuitive desire to achieve additional coarse-graining in the time domain, temporal averaging plays an important role in removing orientational singularities from the phase-specific Eulerian seepage flux relation as written for averaged velocities. Thereby, one ultimately obtains *orientation-independent* error bounds in the formulas for the time-averaged superficial seepage flux (mass per unit superficial area per unit time):

$$\frac{1}{S} \boldsymbol{m}^{(\mathcal{F})} = \rho^{(\mathcal{F})} \boldsymbol{n} \cdot \langle \langle \boldsymbol{u}^{(\mathcal{F})} \rangle_\tau \rangle_t [\Phi^{(\mathcal{F})}]^{-1} + \mathcal{O}[(\ell/\sqrt{S})^{1/2}]$$

$$\frac{1}{S} \boldsymbol{m}^{(\mathcal{P})} = \rho^{(\mathcal{P})} \boldsymbol{n} \cdot \langle \langle \boldsymbol{u}^{(\mathcal{P})} \rangle_\tau \rangle_t [\Phi^{(\mathcal{P})}]^{-1} + \mathcal{O}[(\ell/\sqrt{S})^{1/2}] \tag{16}$$

where ℓ is a characteristic pore scale (e.g., b or L) and $\sqrt{S}$ is a characteristic linear dimension of the surface element used to define the seepage fluxes. Here, $\rho^{(\,)}$ stands for the superficial density of the phase in question (mass per unit total volume of the multiphase mixture). In particular, the kinematic interpretation, Eq. 16, is precisely what is needed in general to justify using the averaged velocities, Eq. 15, in the manner implicit in the macroscopic, phenomenological approach to particulate transport in porous media (Tien and Payatakes, 1979; Sharma and Yortsos, 1987a).

Finally, it should be noted that on time average the spherical particles move along the centerline more than twice as fast as the fluid–particle mixture as a whole, Table 3, even accounting for the retarding wall effects. For the above case we have the dimensionless time-average velocity $\langle v_1 \rangle_t = 0.500$ for the spheres, vs. $\langle \langle u^{(\mathcal{F}\cup\mathcal{P})} \rangle_\tau \rangle_t = 0.230$ for fluid and particles considered together.

An estimate of mean particle velocities based upon hydraulic radius

It would be of interest for obtaining effective phenomenological coefficients to estimate the ratio $\langle v_1 \rangle_t / \langle \langle u^{(\mathcal{F}\cup\mathcal{P})} \rangle_\tau \rangle_t$ without having to explicitly follow the spheres through different positions and subsequently form the time-average quantities. For the purpose of making an approximate calculation, one could conceive of using the time-average velocities of centerline *fluid elements* in *single-phase* flow through a corrugated capillary, Table 3, together with a wall-effect correction factor (accounting for finite particle size) estimated by using a cylindrical tube of the appropriate hydraulic radius.

With the results from previous sections in hand, we are in a position to assess the accuracy of this kind of approximation in a specific case. For a sinusoidal tube characterized by dimensionless inner radius $b = 0.6$ and wavelength $2L = 2.0$, Eq. 1, the mean surface area per volume is matched by a cylindrical tube of radius $R^* = 0.7552$. To use the tabulations of Wang and Skalak (1969), one must then adjust the geometric parameters to the new radius R^*:

$$\alpha^* = \alpha/R^* = 0.3/0.7552 = 0.3972$$
$$2\mathcal{L}^* = 2\mathcal{L}/R^* = 2.0/0.7552 = 2.648$$

Interpolation gives for the approximate, mean wall-effect correction factor $[2U/V](\alpha^*)/2 = 0.8968$. Applying this factor to the ratio $\langle u_z\{r = 0\} \rangle_t^0 / \langle u \rangle_\tau^0 = 2.412$, listed for single-phase flow in Table 3, then yields the value 2.16, which is very close to the result $\langle v_1 \rangle_t / \langle \langle u^{(\mathcal{F}\cup\mathcal{P})} \rangle_\tau \rangle_t = 2.17$ obtained in the previous subsection from detailed calculations.

Dumbbells Moving within Sinusoidal Capillaries: A Model for Polymer Transport in Porous Media

Polymers (e.g., the rodlike polysaccharide xanthan) are used for mobility control in enhanced oil recovery in order to minimize viscous fingering of the displacing fluid; situations in which the macromolecular dimensions are appreciable compared with those of the surrounding pores are of interest in such applications (Gogarty, 1967; Chauveteau, 1982). The singularity method developed here permits detailed modeling of a hydrodynamic hindrance effect. Although a more comprehensive study will be the subject of a subsequent publication, we present here an illustrative calculation.

Polymer molecules are frequently idealized as flexible or rigid

dumbbells (Bird et al., 1987). Neglect of bead–bead and/or bead–wall hydrodynamic interactions—implicit in the characterization of each end by a configuration- and position-independent hydrodynamic friction coefficient—represents a widely used approximation, which is motivated in part by the difficulty of calculating the requisite hydrodynamic coefficients. Thus, the ability to treat the full hydrodynamic problem in complicated dumbbell-pore geometries should prove useful in a variety of applications.

In their analysis of macromolecular orientation during flow through a packed bed (for hydrodynamic chromatography of xanthan), Prud'homme and Hoagland (1983) proposed using a rigid dumbbell within a periodically constricted tube. To model the effects of elongational flow they combined infinite-fluid hydrodynamics of the dumbbell in a steady elongational flow field with an estimate of the local rate of strain derived from the collocation solution of Neira and Payatakes (1978) for single-phase flow in a periodically constricted capillary. Wall shear was treated in an analogous manner, but with the shear rate estimated from an equivalent capillary bundle. Judicious approximations of this kind can lead to useful insights into pore-scale mechanisms; nevertheless it would be most desirable to be able to calculate actual hydrodynamic coefficients for nonspherical particulate or macromolecular models as functions of position and orientation in nonrectilinear pores.

Below we consider in detail a hydrodynamic mobility-reduction effect, which can be illustrated (in the present axisymmetric context) using a rigid-dumbbell model with spherical—not just point-size—ends; all particle–particle and particle–wall interactions are accounted for in the numerical solution.

We refer to the same pore geometry as in the previous calculation ($b = 0.6$, $L = 1$), with both spheres of radius $\alpha_1 = \alpha_2 = 0.3$; see Figure 5. Of course, a dumbbell cannot be regarded *literally* as a model of an actual macromolecule. Nevertheless, it illustrates a salient feature of interest in mobility reduction, namely the additional dissipation observed when rigidly connected hydrodynamic entities are immersed in an otherwise undisturbed flow field which would tend to deform the dumbbell in the absence of a rigid connection between its ends.

Although this effect exists in the rheological context of an effectively unbounded extensional flow field (or when macromolecular dimensions are very small compared to the scale of surfaces bounding the suspending fluid), the case where pore irregularities are of dimensions similar to the dumbbell length should be of interest for practical applications involving polymers in porous media (Gogarty, 1967; Chauveteau, 1982). Here, the dimensionless center-to-center distance is unity. Thus, when $\varphi = 0.25, 0.75$, one sphere is centered in the pore throat whereas the other is centered in the pore body, Figure 5. Correspondingly, the rigid dumbbell resists stretching and compression. Figure 4a shows the normalized total flow rate Q/Q_0 as a function of φ, whereas Figure 6a shows the corresponding values of rod tension T experienced by the dumbbell. (Here, computations need only be carried out for $0 \le \varphi \le 0.25$ because all configuration-specific hydrodynamic quantities must be either even or odd about $\varphi = 0.00, 0.25, 0.50$.)

In order to better understand the overall flow resistance effect associated with suspended dumbbells, we carry out for each geometrical configuration φ_i an analogous computation assuming that the two spherical ends are *freely suspended in their instantaneous positions*. This corresponds conceptually to loosening the sphere–sphere connection in order to decompose the total flow resistance into two classes of hydrodynamic contributions:

- *Independent resistance effect,* due to the purely hydrodynamic interactions occurring between the two spheres and between each and the corrugated walls, assuming that the spheres are not mechanically joined
- *Linkage effect,* which quantifies the increased flow hindrance attributable to the fact that the spheres are rigidly connected, and hence incapable of moving independently.

These values (expressed as percent reductions of the total flow rate) are displayed in Figure 6b. In this example, the instantaneous flow hindrance is dominated by the linkage effect around $\varphi = 0.25, 0.75$, at which freely suspended beads would move with different velocities. At $\varphi = 0.0, 0.5$, freely suspended beads would (by symmetry) move at the same velocity, whence the linkage effect vanishes; the independent resistance effect now attains its maximum value, since both spheres possess the

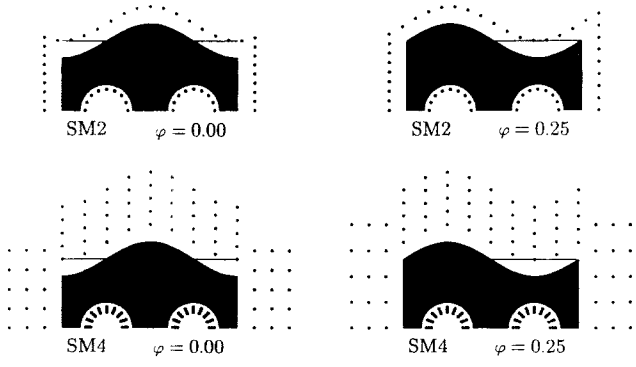

Figure 5. Motion of dumbbells along axis of a sinusoidal pore.
Singularity locations for calculation parameters SM2, SM4 (Table 1) are shown for two geometric configurations

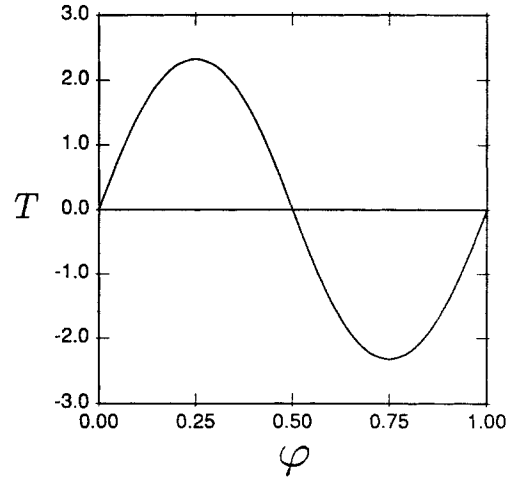

Figure 6. Configuration-specific hydrodynamic quantities for freely suspended dumbbells.
(a) Dimensionless rod tension T vs. φ for $\Delta p_0 = -10.0$.

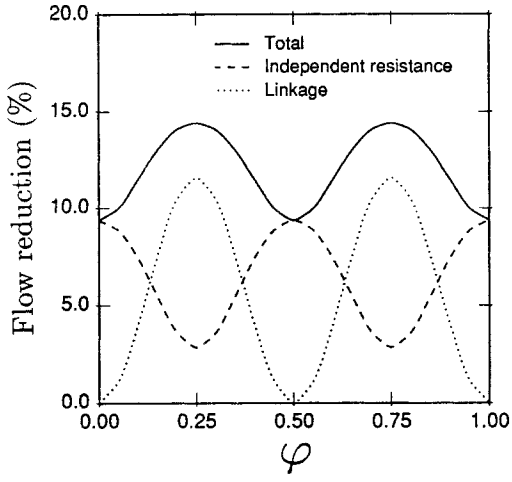

Figure 6b. Decomposition of overall flow hindrance associated with suspended dumbbells into two hydrodynamic submechanisms, independent resistance and linkage.

greatest velocity component normal to the nearby walls. In this example the linkage effect is an important factor in the hydrodynamic mobility reduction. The numerical simulations enable a thought experiment that would otherwise seem to be nearly impossible to duplicate in an actual physical system.

Flexible dumbbells would entail a *nonlinear* problem, with determination of the dumbbell conformation required along with the hydrodynamic flow fields as part of the solution. Nevertheless, the above type of approach appears potentially useful for obtaining upper and lower bounds for the flow parameters as functions of the spring constant, although history dependence would complicate the interpretations.

Conclusions

This paper has explored use of the singularity approach for numerical modeling of particulate hydrodynamics within sinusoidal pores. Results for the test problems considered here demonstrate the accuracy and versatility of the numerical method. The calculations presented in the final sections indicate the type of analysis needed to implement closure for a special class of time-periodic microphenomena, which capture important features of the physics operative in particulate and macromolecular transport processes in porous media.

The suitability of singularity methods for tracking the (quasistatic) evolution of irregularly shaped interstitial geometries stems partly from the fact that although typical pore–particle combinations can lead to complicated shapes for the fluid domain, the domain exterior to the fluid may nevertheless be composed of simply shaped subregions—hence the advantage of using basis functions centered *outside* the fluid domain. The numerical approach avoids the evaluation of singular integrals (and attendant difficulties in evaluating derivatives at the boundary) associated with boundary elements, but can still be implemented to take advantage of the lower dimensional discretization (Mathon and Johnston, 1977; Han and Olson, 1987). Moreover, appropriate clustering of singularities inside particles (Dabros, 1985) can lend a multipole-like character to the method.

For the axisymmetric flow problems considered, both lineal and areal distribution of singularities give good results, although the former is easier to implement and seems less prone to ill conditioning of the least-squares matrix. Mesh refinement should preserve the positions of all singularities already present; here we used an interval-halving algorithm for this purpose.

For a lineal distribution of poles, good results were obtained using roughly even spacing around the boundary; the dimensionless distance between the singularities and the unit cell boundaries was about 0.2, while the particle singularities were located $1/5$ radius in from the sphere surface(s). More relevant information regarding positioning of singularities can be found in Mathon and Johnston (1977), Patterson et al. (1985), and Han and Olson (1987). Further study will be directed toward systematic optimization of the above numerical parameters as well as considerations of selective mesh refinement, for example, by adaptive or heuristic means.

Timed calculation runs were carried out on a Sun SPARCstation 1, using a timing feature of the UNIX operating system. Table 1 lists the computation times for various sets of parameters. Each (single-phase flow) calculation for the SM1 parameters required less than 2 min user time. For the two-sphere calculations using SM2 parameters, computation times were less than 6 min per geometric configuration φ_i.

The particulate flow problems discussed here would appear to be much more difficult from the perspective of numerical grid generation (Thompson et al., 1985), particularly because of the changing geometry. Extensions to fluid–fluid systems would entail separate distributions of singularities for each fluid domain, the respective coefficients ultimately being coupled through the boundary conditions. As an alternative to iterative, boundary-fitted-mesh finite-difference schemes (Ryskin and Leal, 1984), the above advantages should then be useful in solving free-boundary Stokes flow problems, such as arise in bubble or droplet deformation.

Acknowledgment

The authors thank Johannes M. Nitsche and David C. Guell for useful discussions. Suggestions from anonymous refrees were appreciated. This research was supported by grants from the National Science Foundation and the U.S. Army Research Office.

Notation

A = coefficient of parabolic velocity profile $U(r)$
a = radius of hypothetical ghost cylinder for parabolic velocity profile $U(r)$
B_n = coefficient vector for least-squares solution: $\{B_n\} = \{G_n^{[i]}, A\}$
b = minimum radius of sinusoidal tube (maximum radius normalized to unity)
$\mathcal{C}$ = normalization constant in time average over one period
e_z = unit vector in $+z$ direction
$\mathcal{F}$ = weighting factor in summations
F_k = external force exerted in axial direction upon kth particle
$(f_r^{[i]})_j, (f_z^{[i]})_j$ = radial and axial velocity components at $(r, 0, z)$ due to ith type of singularity ($i = 1, 2, 3$) at $(r_n \cos \phi_j, r_n \sin \phi_j, z_n)$
f = vector strength of a Stokeslet (point force solution)
$G_n^{[i]}$ = coefficient of ith type of singularity at nth singularity point

$g_j^{[i]}$ = pressure disturbance at $(r, 0, z)$ due to ith type of singularity at $(r_n \cos \phi_j, r_n \sin \phi_j, z_n)$

G_{V0} = pressure gradient coefficient for freely suspended spheres within a circular cylindrical tube

h = strength of point source

I = idemfactor

J = number of azimuthal subdivisions of interval $[0, \pi]$

K = number of particles

K_U = drag coefficient for sedimenting spheres within a circular cylindrical tube

K_V = drag coefficient for flow past stationary spheres within a circular cylindrical tube

$\mathcal{L}$ = half-length of unit cell τ; $\mathcal{L} = \mathcal{N}L$

L = half-wavelength of sinusoidal tube corrugations

M = number of points at which boundary conditions are imposed on the generating curve of an axisymmetric surface (tube wall, end-cap, particle surface)

M_{row} = number of rows of least-squares rectangular coefficient matrix; $M_{row} = 2M^{(\mathcal{W})} + 5M^{(\mathcal{E})} + 2\sum_{k=1}^{k} M^{(\mathcal{P}_k)}$

$\boldsymbol{m}$ = time-averaged mass flux across an arbitrarily oriented surface element of dimensions much larger than the linear pore scale

$\mathcal{N}$ = number of wavelengths within one unit cell τ

N = total number of singularity points

N_{axis} = number of singularity points lying along axis $z = 0$

N_{col} = number of columns of least-squares rectangular coefficient matrix; $N_{col} = 3N + 1 - N_{axis}$

$p^{\pm}$ = pressure at $\mathcal{S}^{\pm}$ face ($z = \pm\mathcal{L}$) of unit cell τ

Δp_0 = pressure difference $p^+ - p^-$ imposed across unit cell τ

$\Delta P_{\uparrow}^*$ = dimensionless pressure drop across one unit cell in nondimensionalization of Tilton and Payatakes (1984)

$\mathcal{P}_k$ = kth (spheroidal) particle

$p^{[i]}$ = pressure disturbance field due to ith; $p^{[i]} = p^{[i]}(r, z, r_n, z_n)$

P_U = pressure drop coefficient for sedimenting spheres within a circular cylindrical tube

P_V = pressure drop coefficient for flow past stationary spheres within a circular cylindrical tube

Q = volumetric flow rate of fluid (in $+z$ direction) across cell face $\mathcal{S}^+$ (or $\mathcal{S}^-$)

Q_0 = volumetric flow rate through tube in the absence of particles

$\boldsymbol{q} = (r - r_n \cos \phi, -r_n \sin \phi, z - z_n)$

$q = \|\boldsymbol{q}\| = [r^2 + r_n^2 - 2rr_n \cos \phi + (z - z_n)^2]^{1/2}$

$q_{j,n} = [r^2 + r_n^2 - 2rr_n \cos \phi_j + (z - z_n)^2]^{1/2}$

R^* = equivalent radius of a cylindrical pore with the same surface-to-volume ratio as the mean value for the corrugated tube

$R(z)$ = wall function specifying sinusoidal tube shape

r = radial coordinate in circular cylindrical coordinates

Δr = r spacing of end-cap summation points

r_1^*, r_2^* = minimum, maximum tube radii in nondimensionalization of Tilton and Payatakes (1984)

r_n = radial coordinate of nth ring singularity

$r_m^{(\mathcal{W})}, r_m^{(\mathcal{E})}, r_m^{(\mathcal{P}_k)}$ = radial coordinate of mth boundary summation point (on tube wall, end-cap, kth particle surface)

S = area of macroscopic surface element in Eulerian flux relation

$\mathcal{S}^{(\mathcal{W})}$ = tube wall inside unit cell τ

$\mathcal{S}^{\pm}$ = end face of unit cell ($z = \pm\mathcal{L}$)

$\mathcal{S}^{(\mathcal{P}_k)}$ = surface of kth particle in unit cell τ

t = time

$U(r)$ = parabolic velocity profile (regular solution)

$\boldsymbol{u}$ = fluid velocity vector

u_r, u_z = r, z velocity components

$\langle u \rangle_\tau^0$ = volume-average (axial) fluid velocity for single-phase flow through a sinusoidal capillary

$\langle u^{(\mathcal{F})} \rangle_\tau(\varphi)$ = configuration-specific, volume-average velocity of fluid phase

$\langle u^{(\mathcal{P})} \rangle_\tau(\varphi)$ = configuration-specific, volume-average velocity of particulate phase

$\langle u^{(\mathcal{F} \cup \mathcal{P})} \rangle_\tau(\varphi)$ = configuration-specific, volume-average velocity of fluid–particle mixture

v_k = velocity (in axial direction) of kth particle $\mathcal{P}_k$

$v_r^{[i]}, v_z^{[i]}$ = r, z velocity disturbance fields due to ith type of ring singularity ($i = 1, 2, 3$)

$(V_r^{(\mathcal{W})})_{m,n}, (V_z^{(\mathcal{W})})_{m,n}$ = r, z velocity disturbances at $(r_m^{(\mathcal{W})}, z_m^{(\mathcal{W})})$ due to (renumbered) nth singularity

$(V_r^{(\pm)})_{m,n}, (V_z^{(\pm)})_{m,n}$ = r, z velocity disturbances at $(r_m^{(\mathcal{E})}, \pm\mathcal{L})$ due to (renumbered) nth singularity

$(V_r^{(',\pm)})_{m,n}, (V_z^{(',\pm)})_{m,n}$ = z derivatives of above quantities

$(V_r^{(\mathcal{P}_k)})_{m,n}, (V_z^{(\mathcal{P}_k)})_{m,n}$ = r, z velocity disturbances at $(r_m^{(\mathcal{P}_k)}, z_m^{(\mathcal{P}_k)})$ due to (renumbered) nth singularity

$\mathcal{V}_k$ = volume of kth particle

x_n, x_n^0 = shorthand notation for the sets of arguments $\{r, z, r_n, z_n\}, \{r, z, 0, z_n\}$

z = axial coordinate in circular cylindrical coordinates

z_k^c = axial coordinate of kth particle center

$z_m^{(\mathcal{W})}, z_m^{(\mathcal{P}_k)}$ = axial coordinate of mth wall boundary summation point (on tube wall, kth particle surface)

z_n = axial coordinate of nth ring singularity

Greek letters

α_k = axial half-length of spheroidal particle $\mathcal{P}_k$

β_k = radial dimension of spheroidal particle $\mathcal{P}_k$

θ = polar angle in spherical polar coordinates centered about a particle center

$\rho^{(\,)}$ = superficial density of a phase

ρ_m = weight assigned to boundary point (r_m, z_m) in least-squares optimization

ϕ = azimuthal angle

$\Phi^{(\,)}$ = fraction of pore space occupied by a phase

φ = geometric phase variable specifying axial position of sinusoidal tube wall corrugations

τ = unit cell of multiphase system: $\tau = \{(r, z): 0 \le r \le R(z), -\mathcal{L} \le z \le \mathcal{L}\}$

Superscripts

$(\mathcal{E})$ = end caps ($z = \pm\mathcal{L}$)

$(\mathcal{F})$ = fluid phase

$[i]$ = ith type of singularity

$(\mathcal{P})$ = particulate phase

$(\mathcal{P}_k)$ = particle $\mathcal{P}_k$

$(\mathcal{W})$ = tube wall

$\pm$ = pertaining to $z = \pm\mathcal{L}$ face (end cap) of unit cell τ

$*$ = pertaining to equivalent cylindrical pore with same surface-to-volume ratio as the mean value characterizing the corrugated pore

Subscripts

j = index of azimuthal subdivisions around the ring for a ring singularity

k = index of particles

m = index of boundary summation points

n = index of singularity points

Special symbols

$\langle\ \rangle_t$ = time average (over one period T) of a time-periodic function

$\langle\ \rangle_\tau$ = volume average over unit cell τ

Literature Cited

Batchelor, G. K., "Slender-Body Theory for Particles of Arbitrary Cross-Section in Stokes Flow," *J. Fluid Mech.*, **44,** 419 (1970).

Bird, R. B., C. F. Curtiss, R. C. Armstrong, and O. Hassager, *Dynamics of Polymeric Liquids. Vol. 2, Kinetic Theory,* 2d ed., Wiley, New York (1987).

Brenner, H., "Dispersion Resulting from Flow Through Spatially Periodic Porous Media," *Phil. Trans. R. Soc. Lond.*, **A297,** 81 (1980).

Brenner, H., and L. J. Gaydos, "The Constrained Brownian Movement of Spherical Particles in Cylindrical Pores of Comparable Radius. Models of the Diffusive and Convective Transport of Solute Molecules in Membranes and Porous Media," *J. Colloid Interface Sci.*, **58,** 312 (1977).

Chauveteau, G., "Rodlike Polymer Solution Flow Through Fine Pores: Influence of Pore Size on Rheological Behavior," *J. Rheol.*, **26,** 111 (1982).

Chwang, A. T., "Hydromechanics of Low-Reynolds-Number Flow. 3: Motion of a Spheroidal Particle in Quadratic Flows," *J. Fluid Mech.*, **72,** 17 (1975).

Chwang, A. T., and T. Y.-T. Wu, "Hydromechanics of Low-Reynolds-Number Flow. 2: Singularity Method for Stokes Flows," *J. Fluid Mech.*, **67,** 787 (1975).

Corapcioglu, M. Y., N. M. Aboud, and A. Haridas, "Governing Equations for Particle Transport in Porous Media," *Advances in Transport Phenomena in Porous Media,* J. Bear, M. Y. Corapcioglu, eds., 269, NATO ASI Series E: Applied Sciences, No. 128 (1987).

Dąbroś, T., "A Singularity Method for Calculating Hydrodynamic Forces and Particle Velocities in Low-Reynolds-Number Flows," *J. Fluid Mech.*, **156,** 1 (1985).

Deen, W. M., "Hindered Transport of Large Molecules in Liquid-Filled Pores," *AIChE J.*, **33,** 1409 (1987).

Deiber, J. A., and W. R. Schowalter, "Flow Through Tubes with Sinusoidal Axial Variations in Diameter," *AIChE J.*, **25,** 638 (1979).

———, "Modeling the Flow of Viscoelastic Fluids Through Porous Media," *AIChE J.*, **27,** 912 (1981).

Dongarra, J. J., J. R. Bunch, C. B. Moler, and G. W. Stewart, *LINPACK Users' Guide,* Society for Industrial and Applied Mathematics (SIAM), Philadelphia (1979).

Drew, D. A., "Averaged Field Equations for Two-Phase Media," *Stud. Appl. Math.*, **L,** 133 (1971).

Fedkiw, P., and J. Newman, "Mass Transfer at High Péclet Numbers for Creeping Flow in a Packed-Bed Reactor," *AIChE J.*, **23,** 255 (1977).

Giordano, R. M., and J. C. Slattery, "Stability of Static Interfaces in a Sinusoidal Capillary," *J. Colloid Interface Sci.*, **92,** 13 (1983).

———, "Effect of Interfacial Viscosities upon Displacement in Sinusoidal Capillaries," *AIChE J.*, **33,** 1592 (1987).

Gluckman, M. J., R. Pfeffer, and S. Weinbaum, "A New Technique for Treating Multiparticle Slow Viscous Flow: Axisymmetric Flow Past Spheres and Spheroids," *J. Fluid Mech.*, **50,** 705 (1971).

Gogarty, W. B., "Mobility Control with Polymer Solutions," *Soc. Pet. Eng. J.*, **7,** 161 (1967).

Han, P. S., and M. D. Olson, "An Adaptive Boundary Element Method," *Int. J. Numer. Meth. in Eng.*, **24,** 1187 (1987).

Happel, J., and H. Brenner, *Low Reynolds Number Hydrodynamics,* Martinus Nijhoff, Boston (1983).

Hasimoto, H., "On the Periodic Fundamental Solutions of the Stokes Equations and Their Application to Viscous Flow Past a Cubic Array of Spheres," *J. Fluid Mech.*, **5,** 317 (1959).

Hoagland, D. A., and R. K. Prud'homme, "Taylor-Aris Dispersion Arising from Flow in a Sinusoidal Tube," *AIChE J.*, **31,** 236 (1985).

Jiang, T.-S., M. H. Kim, V. J. Kremesec Jr., and J. C. Slattery, "The Local Volume-Averaged Equations of Motion for a Suspension of Non-Neutrally Buoyant Spheres," *Chem. Eng. Commun.*, **50,** 1 (1987).

Karrila, S. J., and S. Kim, "Integral Equations of the Second Kind for Stokes Flow: Direct Solution for Physical Variables and Removal of Inherent Accuracy Limitations," *Chem. Eng. Commun.*, **82,** 123 (1989).

Levich, V. G., *Physicochemical Hydrodynamics,* Prentice-Hall, Englewood Cliffs, NJ (1962).

McAuliffe, C. D., "Oil-in-Water Emulsions and Their Flow Properties in Porous Media," *J. Pet. Tech.*, **25,** 727 (1973).

McHugh, A. J., "Particle Size Measurement Using Chromatography," *Crit. Rev. Anal. Chem.*, **15**(1), 63 (1984).

Mathon, R., and R. L. Johnston, "The Approximate Solution of Elliptic Boundary-Value Problems by Fundamental Solutions," *SIAM J. Numer. Anal.*, **14,** 638 (1977).

Neira, M. A., and A. C. Payatakes, "Collocation Solution of Creeping Newtonian Flow Through Periodically Constricted Tubes with Piecewise Continuous Wall Profile," *AIChE J.*, **24,** 43 (1978).

Nitsche, L. C., "Multiphase Flow Through Spatially Periodic Models of Porous Media," Ph.D. Diss., Dept. Chem. Eng., Mass. Inst. Technology (1989).

Nitsche, L. C., and H. Brenner, "Eulerian Kinematics of Flow Through Spatially Periodic Models of Porous Media," *Arch. Rational Mech. Anal.*, **107,** 225 (1989).

Patterson, C., M. A. Sheikh, and R. P. Scholfield, "On the Application of the Indirect Discrete Method for Three-Dimensional Design Problems," *BETECH 85. Proc. 1st Boundary Element Tech. Conf., South Australian Inst. of Tech., Adelaide, Australia, Nov. 1985,* C. A. Brebbie, B. J. Noye, eds., Computational Mechanics Pubs., Springer, New York (1985).

Payatakes, A. C., and M. A. Neira, "Model of the Constricted Unit Cell Type for Isotropic Granular Porous Media," *AIChE J.*, **23,** 922 (1977).

Payatakes, A. C., C. Tien, and R. M. Turian, "A New Model for Granular Porous Media. I: Model Formulation," *AIChE J.*, **19,** 58 (1973); "II: Numerical Solution of Steady State Incompressible Newtonian Flow Through Periodically Constricted Tubes," *ibid.*, 67 (1973).

———, "Trajectory Calculation of Particle Deposition in Deep Bed Filtration. I: Model Formulation," *AIChE J.*, **20,** 889 (1974); "II: Case Study of the Effect of the Dimensionless Groups and Comparison with Experimental Data," *ibid.*, 900 (1974).

Phan-Thien, N., and M. M. K. Khan, "Flow of an Oldroyd-Type Fluid Through a Sinusoidally Corrugated Tube," *J. Non-Newtonian Fluid Mech.*, **24,** 203 (1987).

Press, W. H., B. P. Flannery, S. A. Teukolsky, and W. T. Vetterling, *Numerical Recipes. The Art of Scientific Computing,* Cambridge Univ. Press, New York (1986).

Prud'homme, R. K., and D. A. Hoagland, "Orientation of Rigid Macromolecules During Hydrodynamic Chromatography Separations," *Sep. Sci. Tech.*, **18,** 121 (1983).

Ryskin, G., and L. G. Leal, "Numerical Solution of Free-Boundary Problems in Fluid Mechanics. 1: The Finite-Difference Technique," *J. Fluid Mech.*, **148,** 1 (1984); "2: Buoyancy-Driven Motion of a Gas Bubble Through a Quiescent Liquid," *ibid.*, 19 (1984); "3: Bubble Deformation in an Axisymmetric Straining Flow," *ibid.*, 37 (1984).

Sáez, A. E., R. G. Carbonell, and J. Levec, "The Hydrodynamics of Trickling Flow in Packed Beds: I. Conduit Models," *AIChE J.*, **32,** 353 (1986).

Sangani, A. S., and A. Acrivos, "Slow Flow Through a Periodic Array of Spheres," *Int. J. Multiphase Flow,* **8,** 343 (1982).

Scheidegger, A. E., *The Physics of Flow Through Porous Media,* 3rd ed., Univ. Toronto Press, Buffalo (1974).

Schmidt, D. P., H. Soo, and C. J. Radke, "Linear Oil Displacement by the Emulsion Entrapment Process," *Soc. Pet. Eng. J.*, **24,** 351 (1984).

Sharma, M. M., and Y. C. Yortsos, "Transport of Particulate Suspensions in Porous Media: Model Formulation," *AIChE J.*, **33,** 1636 (1987a).

———, "A Network Model for Deep Bed Filtration Processes," *AIChE J.*, **33,** 1644 (1987b).

———, "Fines Migration in Porous Media," *AIChE J.*, **33,** 1654 (1987c).

Thompson, J. F., Z. U. A. Warsi, and C. W. Mastin, *Numerical Grid Generation. Foundations and Applications,* North-Holland, New York (1985).

Tien, C., and A. C. Payatakes, "Advances in Deep Bed Filtration," *AIChE J.*, **25,** 737 (1979).

Tilton, J. N., and A. C. Payatakes, "Collocation Solution of Creeping Newtonian Flow Through Sinusoidal Tubes: A Correction," *AIChE J.*, **30,** 1016 (1984).

Wang, H., and R. Skalak, "Viscous Flow in a Cylindrical Tube Containing a Line of Spherical Particles," *J. Fluid Mech.*, **38,** 75 (1969).

Whitaker, S., "The Transport Equations for Multiphase Systems," *Chem. Eng. Sci.*, **28**, 139 (1973).
———, "Flow in Porous Media. II: The Governing Equations for Immiscible, Two-Phase Flow," *Transport in Porous Media*, **1**, 105 (1986).
Youngren, G. K., and A. Acrivos, "Stokes Flow Past a Particle of Arbitrary Shape: A Numerical Method of Solution," *J. Fluid. Mech.*, **69**, 377 (1975).
Zick, A. A., and G. M. Homsy, "Stokes Flow Through Periodic Arrays of Spheres," *J. Fluid Mech.*, **115**, 13 (1982).

Appendix A: Evaluation of Singular Ring Solutions

We ultimately seek an axisymmetric solution in the form $u_z(r, z)$, $u_r(r, z)$, $p(r, z)$. However, for purposes of constructing the ring singularities it is convenient to revert momentarily to cartesian coordinates in order to compute the flow field at a point $(r, 0, z)$ due to a point disturbance (point force $\boldsymbol{f}$ or point source of strength h) located at $(r_n \cos\phi, r_n \sin\phi, z_n)$:

$$\text{Point force: } \boldsymbol{u} = \frac{1}{8\pi}\left(\frac{1}{q}\boldsymbol{I} + \frac{1}{q^3}\boldsymbol{qq}\right)\cdot \boldsymbol{f}, \quad p = \frac{1}{4\pi}\frac{1}{q^3}\boldsymbol{q}\cdot\boldsymbol{f}$$

$$\text{Point source: } \boldsymbol{u} = \frac{h}{4\pi}\frac{1}{q^3}\boldsymbol{q}, \quad p = 0 \tag{A1}$$

(Dąbroś 1985), where

$$\boldsymbol{q} = (r - r_n\cos\phi, -r_n\sin\phi, z - z_n)$$
$$q = \|\boldsymbol{q}\| = [r^2 + r_n^2 - 2rr_n\cos\phi + (z - z_n)^2]^{1/2} \tag{A2}$$

(Karrila and Kim 1989).

At each position ϕ around the ring the radial-force and axial-force ring singularities are associated with the respective force vectors $(\cos\phi, \sin\phi, 0)$ and $(0, 0, 1)$. In the present implementation, integration of a constant lineal force density around the ring is replaced by a uniformly weighted summation involving the discrete azimuthal positions $\phi_j = j\Delta\phi$, $j = 1, 2, \ldots, 2J$ $(\Delta\phi = \pi/J)$; symmetry allows the sum to be rewritten so as to involve only $j = 0, 1, 2, \ldots, J$ (with $\phi_0 = 0$). The resulting formula corresponds to a trapezoid-rule evaluation of complete elliptic integrals, which gives exponential convergence as the number of subdivisions is increased.

Denote by $v_r^{[i]}$, $v_z^{[i]}$, and $p^{[i]}$ the respective r and z velocity components and the pressure associated with the ith type of ring singularity $(i = 1, 2, 3)$. These are given by the expressions

$$v_r^{[i]}(\boldsymbol{x}_n) = \frac{1}{16\pi J}\sum_{j=0}^{J}\mathcal{F}_j(f_r^{[i]})_j(\boldsymbol{x}_n)$$
$$v_z^{[i]}(\boldsymbol{x}_n) = \frac{1}{16\pi J}\sum_{j=0}^{J}\mathcal{F}_j(f_z^{[i]})_j(\boldsymbol{x}_n)$$
$$p^{[i]}(\boldsymbol{x}_n) = \frac{1}{8\pi J}\sum_{j=0}^{J}\mathcal{F}_j g_j^{[i]}(\boldsymbol{x}_n) \tag{A3}$$

with

$$\mathcal{F}_j = \begin{cases} 1 & j = 0, J \\ 2 & \text{otherwise} \end{cases} \tag{A4}$$

and $\boldsymbol{x}_n$ representing a shorthand notation for the set of arguments $\{r, z, r_n, z_n\}$. A direct computation yields the following formulas (with $q_{j,n} = [r^2 + r_n^2 - 2rr_n\cos\phi_j + (z - z_n)^2]^{1/2}$):

$$(f_r^{[1]})_j(\boldsymbol{x}_n) = \frac{\cos\phi_j}{q_{j,n}} + \frac{(r\cos\phi_j - r_n)(r - r_n\cos\phi_j)}{q_{j,n}^3}$$
$$(f_r^{[2]})_j(\boldsymbol{x}_n) = \frac{(z - z_n)(r - r_n\cos\phi_j)}{q_{j,n}^3}$$
$$(f_r^{[3]})_j(\boldsymbol{x}_n) = 2\frac{r - r_n\cos\phi_j}{q_{j,n}^3} \tag{A5}$$

$$(f_z^{[1]})_j(\boldsymbol{x}_n) = \frac{(r\cos\phi_j - r_n)(z - z_n)}{q_{j,n}^3}$$
$$(f_z^{[2]})_j(\boldsymbol{x}_n) = \frac{1}{q_{j,n}} + \frac{(z - z_n)^2}{q_{j,n}^3}$$
$$(f_z^{[3]})_j(\boldsymbol{x}_n) = 2\frac{z - z_n}{q_{j,n}^3} \tag{A6}$$

$$g_j^{[1]}(\boldsymbol{x}_n) = \frac{r\cos\phi_j - r_n}{q_{j,n}^3}$$
$$g_j^{[2]}(\boldsymbol{x}_n) = \frac{z - z_n}{q_{j,n}^3}$$
$$g_j^{[3]}(\boldsymbol{x}_n) = 0 \tag{A7}$$

Here, $g_j^{[3]} = 0$ because the pressure field associated with the ring source is zero, Eq. A1.

To impose periodicity of the velocity field we also need to obtain formulas for $\partial u_r/\partial z$ and $\partial u_z/\partial z$. These are given by equations analogous to Eqs. 8 and A3 with

$$\left(\frac{\partial}{\partial z}f_r^{[1]}\right)_j(\boldsymbol{x}_n) = -\frac{z - z_n}{q_{j,n}^3}\cdot\left[\cos\phi_j + \frac{3(r\cos\phi_j - r_n)(r - r_n\cos\phi_j)}{q_{j,n}^2}\right]$$
$$\left(\frac{\partial}{\partial z}f_r^{[2]}\right)_j(\boldsymbol{x}_n) = \frac{r - r_n\cos\phi_j}{q_{j,n}^3}\left[1 - \frac{3(z - z_n)^2}{q_{j,n}^2}\right]$$
$$\left(\frac{\partial}{\partial z}f_r^{[3]}\right)_j(\boldsymbol{x}_n) = -6\frac{(r - r_n\cos\phi_j)(z - z_n)}{q_{j,n}^5}, \tag{A8}$$

$$\left(\frac{\partial}{\partial z}f_z^{[1]}\right)_j(\boldsymbol{x}_n) = \frac{r\cos\phi_j - r_n}{q_{j,n}^3}\left[1 - \frac{3(z - z_n)^2}{q_{j,n}^2}\right]$$
$$\left(\frac{\partial}{\partial z}f_z^{[2]}\right)_j(\boldsymbol{x}_n) = \frac{z - z_n}{q_{j,n}^3}\left[1 - \frac{3(z - z_n)^2}{q_{j,n}^2}\right]$$
$$\left(\frac{\partial}{\partial z}f_z^{[3]}\right)_j(\boldsymbol{x}_n) = \frac{2}{q_{j,n}^3}\left[1 - \frac{3(z - z_n)^2}{q_{j,n}^2}\right] \tag{A9}$$

For those singularities lying along the z axis $(r_n = 0)$ we have the simpler formulas (with $q = [r^2 + (z - z_n)^2]^{1/2}$ and

$x_n^0 = \{r, z, 0, z_n\}$)

$$v_r^{[1]}(x_n^0) = 0, \qquad v_z^{[1]}(x_n^0) = 0, \qquad p^{[1]}(x_n^0) = 0$$
$$v_r^{[2]}(x_n^0) = \frac{r(z - z_n)}{8\pi q^3}, \qquad v_z^{[2]}(x_n^0) = \frac{1}{8\pi}\left(\frac{1}{q} + \frac{(z - z_n)^2}{q^3}\right), \qquad p^{[2]}(x_n^0) = \frac{z - z_n}{4\pi q^3} \tag{A10}$$
$$v_r^{[3]}(x_n^0) = \frac{r}{4\pi q^3}, \qquad v_z^{[3]}(x_n^0) = \frac{z - z_n}{4\pi q^3}, \qquad p^{[3]}(x_n^0) = 0$$

and

$$\frac{\partial}{\partial z} v_r^{[1]}(x_n^0) = 0, \qquad \frac{\partial}{\partial z} v_z^{[1]}(x_n^0) = 0,$$
$$\frac{\partial}{\partial z} v_r^{[2]}(x_n^0) = \frac{r}{8\pi q^3}\left[1 - \frac{3(z - z_n)^2}{q^2}\right], \qquad \frac{\partial}{\partial z} v_z^{[2]}(x_n^0) = \frac{z - z_n}{8\pi q^3}\left[1 - \frac{3(z - z_n)^2}{q^2}\right] \tag{A11}$$
$$\frac{\partial}{\partial z} v_r^{[3]}(x_n^0) = -\frac{3r(z - z_n)}{4\pi q^5}, \qquad \frac{\partial}{\partial z} v_z^{[3]}(x_n^0) = \frac{1}{4\pi q^3}\left[1 - \frac{3(z - z_n)^2}{q^2}\right]$$

Appendix B: Algorithm for Least-Squares Boundary Optimization

The boundary points are indexed by m; to each is assigned a weight ρ_m corresponding to Simpson's rule for approximating the axisymmetric integral, Eq. 9. Although the driver program can be used with arbitrary function subprograms prescribing the shape of the tube wall and the particle(s)—along with supporting data—the discussion here is restricted to sinusoidal capillaries and spheroidal particles.

Tube wall, $\mathcal{W}$: $z_m^{(\mathcal{W})} = -\mathcal{L} + (m-1)\Delta z$, $r_m^{(\mathcal{W})} = R(z_m^{(\mathcal{W})})$

$$\rho_m^{(\mathcal{W})} = \mathcal{F}_m 2\pi r_m^{(\mathcal{W})}\{1 + [R'(z_m^{(\mathcal{W})})^2\}^{1/2}\Delta z \tag{B1}$$

with $m = 1, 2, \ldots, M^{(\mathcal{W})}$; $\Delta z = 2\mathcal{L}/(M^{(\mathcal{W})} - 1)$.

End-cap ($z = \mathcal{L}$), $\mathcal{E}$: $r_m^{(\mathcal{E})} = (m-1)\Delta r$, $z_m^{(\mathcal{E})} = \mathcal{L}$

$$\rho_m^{(\mathcal{E})} = \mathcal{F}_m 2\pi r_m^{(\mathcal{E})}\Delta r \tag{B2}$$

with $m = 1, 2, \ldots, M^{(\mathcal{E})}$; $\Delta r = R(\mathcal{L})/(M^{(\mathcal{E})} - 1)$.

Spheroidal particle k, $\mathcal{P}_k$:

$$r_m^{(\mathcal{P}_k)} = \beta_k \sin\theta_m,\ z_m^{(\mathcal{P}_k)} = z_k^c + \alpha_k \cos\theta_m,\ \theta_m = (m-1)\Delta\theta$$
$$\rho_m^{(\mathcal{P}_k)} = \mathcal{F}_m 2\pi\beta_k \sin\theta_m [\alpha_k^2 \sin^2\theta_m + \beta_k^2 \cos^2\theta_m]^{1/2}\Delta\theta$$
$$\text{with } m = 1,2,\ldots,M^{(\mathcal{P}_k)};\Delta\theta = \pi/(M^{(\mathcal{P}_k)} - 1). \tag{B3}$$

(See Karrila and Kim, 1989.) Here, $M^{(\mathcal{W})}$, $M^{(\mathcal{E})}$, and the $M^{(\mathcal{P}_k)}$ must be odd; moreover, the factor $\mathcal{F}_m$ takes on the appropriate value (1/3, 4/3, or 2/3) as required by Simpson's rule.

For compactness of notation in implementing the FORTRAN code we renumber the singularities in the following order:

Type 1 (radial force): $n = 1, 2, \ldots, N$
Type 2 (axial force): $n = N + 1, N + 2, \ldots, 2N$
Type 3 (source): $n = 2N + 1, 2N + 2, \ldots, 3N$ (B4)

Correspondingly, we collect the coefficients $G_n^{[i]}$, A into a $(3N + 1)$-dimensional vector B_n:

$$B_{n+(i-1)N} = G_n^{[i]} \quad (i = 1, 2, 3; \quad n = 1, 2, \ldots, N)$$
$$B_{3N+1} = A \tag{B5}$$

Define the generic symbols V_z, V_r, and p as the disturbance fields produced by the nth singularity (or by the quadratic velocity field) evaluated at the mth boundary summation point:

$$(V_z^{(\mathcal{W})})_{m,n+(i-1)N} = v_z^{[i]}(r_m^{(\mathcal{W})}, z_m^{(\mathcal{W})}, r_n, z_n)$$
$$(V_r^{(\mathcal{W})})_{m,n+(i-1)N} = v_r^{[i]}(r_m^{(\mathcal{W})}, z_m^{(\mathcal{W})}, r_n, z_n)$$
$$(i = 1, 2, 3; \quad m = 1, 2, \ldots, M^{(\mathcal{W})}; \quad n = 1, 2, \ldots, N) \tag{B6}$$

$$(V_z^{(\pm)})_{m,n+(i-1)N} = v_z^{[i]}(r_m^{(\mathcal{E})}, \pm\mathcal{L}, r_n, z_n)$$
$$(V_r^{(\pm)})_{m,n+(i-1)N} = v_r^{[i]}(r_m^{(\mathcal{E})}, \pm\mathcal{L}, r_n, z_n)$$
$$(V_z^{(',\pm)})_{m,n+(i-1)N} = \frac{\partial}{\partial z} v_z^{[i]}(r_m^{(\mathcal{E})}, \pm\mathcal{L}, r_n, z_n)$$
$$(V_r^{(',\pm)})_{m,n+(i-1)N} = \frac{\partial}{\partial z} v_r^{[i]}(r_m^{(\mathcal{E})}, \pm\mathcal{L}, r_n, z_n)$$
$$p^{\pm}_{m,n+(i-1)N} = p^{[i]}(r_m^{(\mathcal{E})}, \pm\mathcal{L}, r_n, z_n)$$
$$(i = 1, 2, 3; \quad m = 1, 2, \ldots, M^{(\mathcal{E})}; \quad n = 1, 2, \ldots, N) \tag{B7}$$

$$(V_z^{(\mathcal{P}_k)})_{m,n+(i-1)N} = v_z^{[i]}(r_m^{(\mathcal{P}_k)}, z_m^{(\mathcal{P}_k)}, r_n, z_n)$$
$$(V_r^{(\mathcal{P}_k)})_{m,n+(i-1)N} = v_r^{[i]}(r_m^{(\mathcal{P}_k)}, z_m^{(\mathcal{P}_k)}, r_n, z_n)$$
$$(k = 1, 2, \ldots, K; \quad i = 1, 2, 3;$$
$$m = 1, 2, \ldots, M^{(\mathcal{P}_k)}; \quad n = 1, 2, \ldots, N) \tag{B8}$$

The following jump quantities are defined with reference to the periodicity and pressure drop conditions (Eqs. 5 and 6,

respectively):

$$
\begin{aligned}
[[V_z]]_{m,n} &= (V_z^{(+)})_{m,n} - (V_z^{(-)})_{m,n} \\
[[V_z']]_{m,n} &= (V_z^{(',+)})_{m,n} - (V_z^{(',-)})_{m,n} \\
[[V_r]]_{m,n} &= (V_r^{(+)})_{m,n} - (V_r^{(-)})_{m,n} \\
[[V_r']]_{m,n} &= (V_r^{(',+)})_{m,n} - (V_r^{(',-)})_{m,n} \\
[[P]]_{m,n} &= p^+_{m,n} - p^-_{m,n} \\
&\qquad (m = 1, 2, \ldots, M^{(\mathcal{E})};\quad n = 1, 2, \ldots, 3N)
\end{aligned} \tag{B9}
$$

The quadratic velocity profile $U(\boldsymbol{r})$ is associated with the function values

$$
\begin{aligned}
W_m^{(\mathcal{W})} &= U(r_m^{(\mathcal{W})}), \quad (m = 1, 2, \ldots, M^{(\mathcal{W})}) \\
W_m^{(\mathcal{E})} &= U(r_m^{(\mathcal{E})}), \quad (m = 1, 2, \ldots, M^{(\mathcal{E})}) \\
W_m^{(\mathcal{P}_k)} &= U(r_m^{(\mathcal{P}_k)}) \quad (m = 1, 2, \ldots, M^{(\mathcal{P}_k)})
\end{aligned} \tag{B10}
$$

In each calculation, we specify the sphere velocities v_k ($k = 1, 2, \ldots, K$) and pressure drop Δp_0. Optimization of the coefficients B_n then leads to a linear least-squares problem, for which we use a LINPACK QR algorithm (Dongarra et al., 1979, chap. 9) to solve the rectangular matrix equation $Xb = y$ (LINPACK routines DQRDC and DQRSL). (In the original study [Nitsche, 1989, chaps. 6 and 7], which led to this paper, the boundary criterion was written as a quadratic form, from which the normal equations [Press et al., 1986, chap. 14] were derived and subsequently solved for the coefficients B_n; this method proved satisfactory for the single-particle computations presented therein.)

Corresponding, respectively, to the collection of all points at which the boundary conditions are stipulated, and to the singularity coefficients, the rectangular matrix X has $M_{row} = 2M^{(\mathcal{W})} + 5M^{(\mathcal{E})} + 2\sum_{k=1}^{K} M^{(\mathcal{P}_k)}$ rows and $N_{col} = 3N + 1 - N_{axis}$ columns. The rows are filled in the order: tube wall, end-cap, particles. For example, for the tube wall we set

$$
\left.
\begin{aligned}
X_{m,n+(i-1)N} &= v_z^{[i]}(\boldsymbol{x}_{m,n})\,[\rho_m^{(\mathcal{W})}]^{1/2} \\
X_{m,3N+1} &= W_m^{(\mathcal{W})}\,[\rho_m^{(\mathcal{W})}]^{1/2} \\
X_{m+M^{(\mathcal{W})},n+(i-1)N} &= v_r^{[i]}(\boldsymbol{x}_{m,n})\,[\rho_m^{(\mathcal{W})}]^{1/2} \\
X_{m+M^{(\mathcal{W})},3N+1} &= 0
\end{aligned}
\right\}
\begin{pmatrix} m = 1, 2, \ldots M^{(\mathcal{W})} \\ n = 1, 2, \ldots, N \\ i = 1, 2, 3 \end{pmatrix}
$$

and

$$
y_m = 0, \quad (m = 1, 2, \ldots, 2M^{(\mathcal{W})})
$$

where $\boldsymbol{x}_{m,n} = (r_m^{(\mathcal{W})}, z_m^{(\mathcal{W})}, r_n, z_n)$.

The calculations reported here were carried out using the sets of parameters listed in Table 1. Mesh refinement for the singular basis functions was done by positioning further singularities *between* those already present in each row (column, arc), and similarly for the rows (columns, arcs) themselves when carrying out a two-dimensional discretization.

For singularities lying on the axis, the radial-force coefficients $G_n^{[1]} = B_n$ play no role in the optimization; the corresponding columns of X are eliminated using a feature of the pivoting option in LINPACK routine DQRDC.

Once the full matrix X has been generated, the FORTRAN program described here carries out a set of least-squares optimizations by introducing particles successively, one at a time, up to to the total number K. In this way results are obtained for the empty tube and for fewer particles without wasting any of the (then already existing) computations for X. For example, some of the results for suspended spheres were obtained as a by-product of the more extensive dumbbell calculations. This feature is also of utility in validating the arrangement of singularities—for example, a comparison of empty-tube calculations with the results of Tilton and Payatakes (1984) for different values of the geometric phase parameter φ.

Manuscript received Sept. 14, 1989, and revision received July 6, 1990.